2007

Probing Isoforms of the Prion Protein through Tyrosine Nitration

Christopher William Lennon
The University of Montana

PROBING ISOFORMS OF THE PRION

PROTEIN THROUGH TYROSINE NITRATION

By

Christopher William Lennon

B.A. Biology, University of Montana, Missoula, MT, 2005
B.A. Social Work, University of Montana, Missoula, MT, 2005

Thesis

presented in partial fulfillment of the requirements
for the degree of

Master of Science
in Biochemistry

The University of Montana
Missoula, MT

Summer 2007

Approved by:

Dr. David A. Strobel, Dean
Graduate School

Dr. Michele A. McGuirl, Chair
Division of Biological Sciences

Dr. D. Scott Samuels
Division of Biological Sciences

Dr. Kent Sugden
Chemistry Department

Lennon, Christopher, M.S., July 2007 *Biochemistry*

Probing Isoforms of the Prion Protein through Tyrosine Nitration

Chairperson: Dr. Michele A. McGuirl

The prion protein (PrP) has multiple stable isoforms. When PrP misfolds, it aggregates and causes neurological disease and death in mammals. The structure of the non-pathogenic isoform has been determined while the structures of the disease related isoforms are unknown. The nitration labeling patterns of three PrP isoforms with peroxynitrite and tetranitromethane, as detected by mass spectrometry, are reported. Two conserved tyrosine residues (tyrosines 149 and 150) are not labeled by either reagent in the normal cellular form of the prion protein but these residues become reactive after the protein has been converted to one of two aggregated isoforms. Another difference observed is that two other conserved tyrosine residues, 225 and 226, are much less reactive in both aggregated isoforms, while all other tyrosine residues show virtually no isoform specific-labeling. Thus, two regions been identified in which Tyr residues undergo a change in solvent accessibility, which may be due to a conformational change in that region or to inter-subunit packing

CHAPTER 1: BACKGROUND AND SIGNIFICANCE

Prion diseases are a class of fatal neurodegenerative disorders. A number of different prion diseases occur in animals including, but not limited to, Creutzfeldt-Jacob disease in humans, mad cow disease in bovines, chronic wasting disease in deer and elk, and scrapie in sheep. Interestingly, prion disorders may be inherited, sporadic or transmissible, a characteristic in nature held only by prion diseases [1].

Prion diseases also belong to the larger category of amyloidoses, which include Alzheimer's, Parkinson's, Huntington's and Amyotrophic Lateral Sclerosis (ALS) diseases. In amyloidoses, misfolded proteins form ordered aggregates in the central nervous system that are associated with characteristic plaque formation and neurodegeneration [2].

The "protein-only" hypothesis of prion replication postulates that an infectious, misfolded oligomeric prion protein particle (the “prion”) causes the normal, non-infectious cellular form of the prion protein (PrP^{C}) to undergo a conformational change. This conversion event leads to the incorporation of PrP^{C} monomers into the infectious particle, referred to as PrP^{Sc} [3].

Currently, the protein-only hypothesis has not been proven. The key missing proof is the generation of infectious prions entirely *in vitro* [4].

However, based upon the available data, the idea has generally been accepted and three studies in particular have provided compelling support of the protein-only hypothesis.

Büeler and co-workers showed that knockout mice who do not express PrP^{C} appear to develop normally and are much less susceptible to PrP^{Sc} infection than wild-type mice [5]. These data strongly suggest that PrP^{C} is needed to propagate the PrP^{Sc} infection. Furthermore, the study found that heterozygous strains expressing less PrP^{C} than usual displayed significant resistance over wild-type mice to disease as well.

Legname and colleagues [6] injected recombinant amyloid fibrils (PrP^{F}) generated from murine PrP (residues 89-230) into transgenic mice overexpressing PrP^{C} of the same sequence and found the formation of prion-like disease. Fibrils isolated from these mice were then able to infect wild-type mice.

Unfortunately, the exact implications of the Legname study are unknown because of problems in the experimental design and results [7]. Most striking is that the strain of mice used overexpress PrP^{C} in such high levels that they are able to develop the disease spontaneously. Also, the infectivity of the recombinant fibrils was much less than that of normal PrP^{Sc}.

Castilla *et al.* [8] have likely provided the most convincing data in support of the protein-only hypothesis through a process called “protein misfolding cyclic amplification” (PMCA), which attempts to mimic normal

PrP^{Sc} propagation *in vitro*. Using a small amount of PrP^{Sc} purified from hamster as a template, the authors generated infectious fibers *in vitro* from PrP^{C} purified from healthy hamster brain homogenate. In order to ensure (as much as possible) that only *in vitro* fibrils were present, serial dilutions were performed. Further supporting the claims of this study, a control group which was inoculated with non-converted PrP^{C} did not develop disease.

The reason that the Castilla *et al.* study does not entirely prove the protein-only hypothesis is that the PrP^{C} from the brain homogenate of healthy hamsters was used. Because this is the case, there is no way to ensure that only PrP^{C} was present for the template PrP^{Sc} to associate with. In other words, there could be some necessary unknown factor, say a virus, present in the brain homogenate.

Inherent in the protein-only hypothesis is that no bacteria or virus is required for infection. More specifically, no DNA or RNA is required to sustain the infection, just a supply of PrP^{C} monomers. This lack of nucleic acid appears to be unique to prion disorders among infectious diseases. However, a recent study suggests that other amyloid protein deposits have the potential to be infectious as well [9]. Mice over-expressing the human Amyloid Precursor Protein became infected with an Alzheimer's like disease following intercranial inoculation with β-amyloid that was isolated from humans with Alzheimer's. In fact, all amyloid diseases appear to share common structural characteristics and are capable of *in*

vitro self propagation (like prions) [10]. Therefore, it is possible that if given the opportunity, other amyloid plaque diseases would be infectious.

To explain the protein-only hypothesis, two models describing how the correctly folded PrP^{C} misfolds to form the pathogenic PrP^{Sc} have been proposed. These two models are known as the refolding model and the seeding model (figure 1-1) [11].

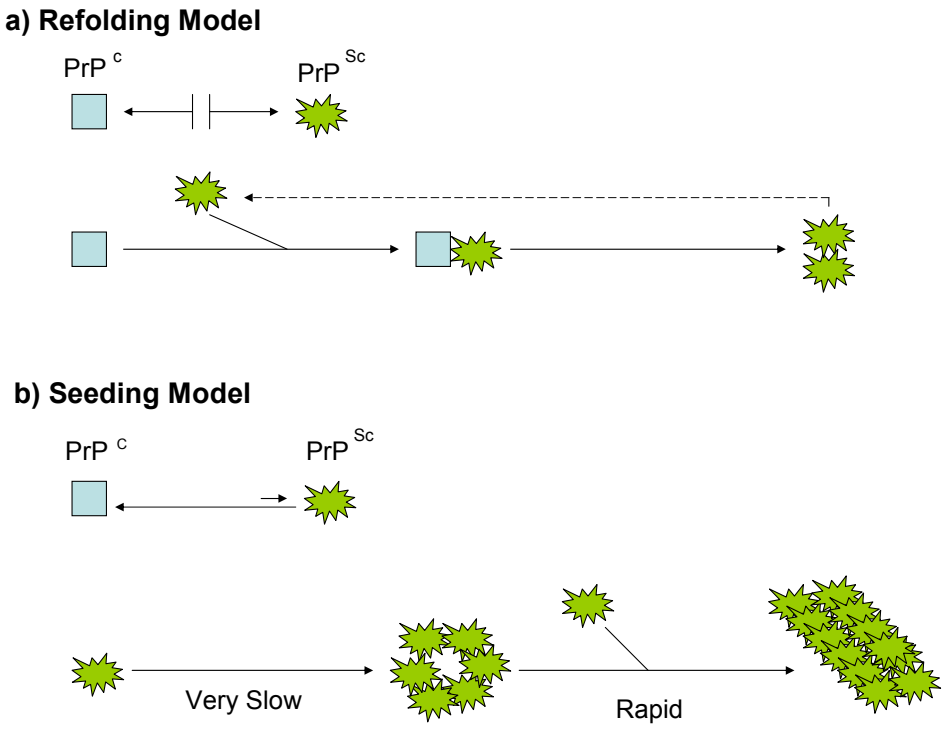

Figure 1-1. Models explaining the protein-only hypothesis (figure adapted from reference 11).

The refolding model states that the conversion of PrP^{C} monomers to PrP^{Sc} is governed by a large activation energy barrier and does not occur at detectable levels. However, upon interaction of PrP^{C} with PrP^{Sc},

either from an exogenous (transmitted) or endogenous (inherited or sporadic) source, PrP^{C} partially unfolds and refolds through association with PrP^{Sc}. Somehow through this unfolding and refolding process, the thermodynamic barrier is able to be overcome.

The seeding model states that PrP^{C} and an oligomeric precursor of PrP^{Sc} are in an equilibrium with one another that highly favors the PrP^{C} isoform. Only when multiple PrP^{Sc} molecules are given a chance to interact with one another is the pathogenic conformation stabilized and the so called seed is able to form. In the case of infection by PrP^{Sc} particles, the seed is what is transmitted. After the seed has been generated, the addition of PrP^{C} monomers to the PrP^{Sc} multimer is rapid.

PrP^{C} is a soluble monomer dominated by α-helical structure while PrP^{Sc} is an isoform enriched in β-sheet that forms insoluble fibrils and is associated with infectivity [1]. PrP^{F} are the recombinant PrP fibers associated with much lower levels of infectivity [4]. Remarkably, no covalent modifications occur during the conversion of PrP^{C} monomers to PrP^{Sc} fibrils; the difference between PrP^{C} and PrP^{Sc} is purely conformational [12]. Furthermore, the prion protein has the ability to form at least one other distinct stable isoform. This third conformer, known as the β-oligomer, is a soluble oligomer of 8-12 subunits that has a similar secondary structure to PrP^{Sc} [13].

High resolution structures of PrP^{C} from numerous mammals have been determined by both NMR (figure 1-2) [14-22] and X-ray

crystallography [23, 24]. In stark contrast, the tendency of all amyloid fibers, including the infectious PrP^{Sc}, to form large heterogeneous aggregates has hampered the elucidation of structural details. Figure 1-3 shows the gross structure and the fibrillar nature of PrP^{F}. No NMR or crystal structures of the β-oligomer currently exist either.

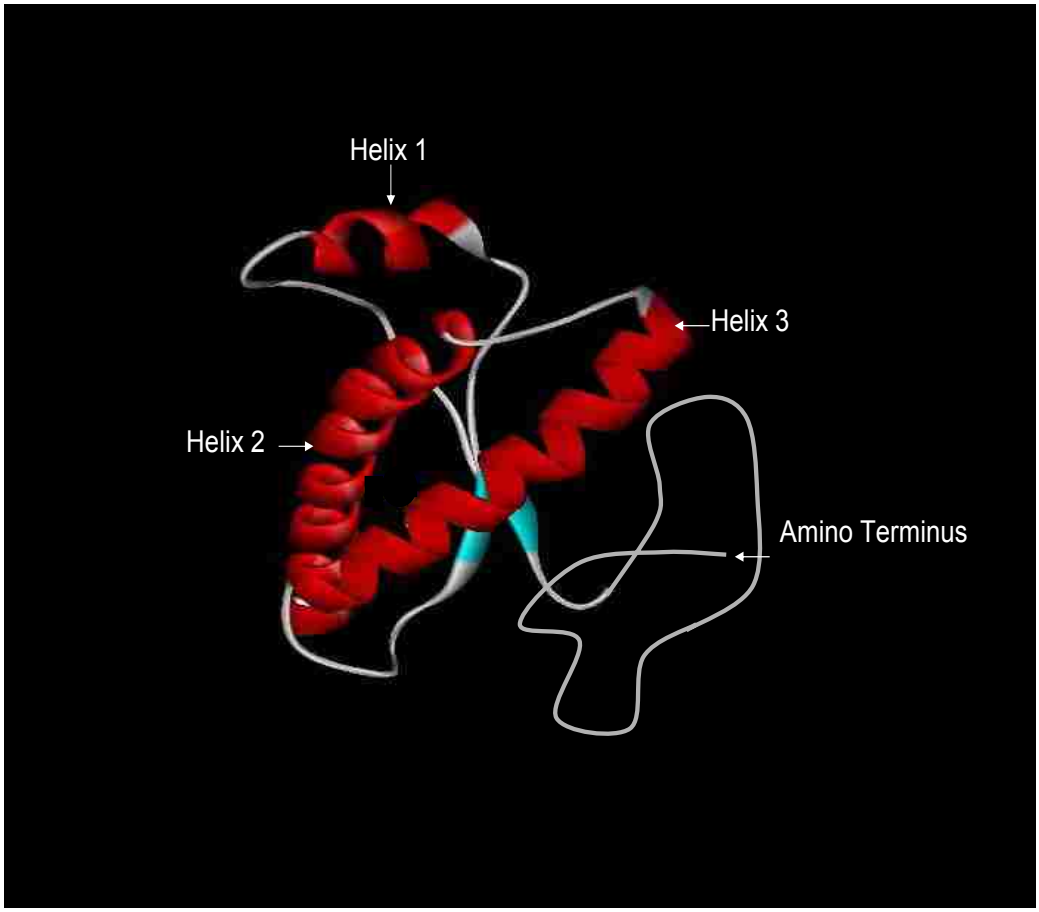

Figure 1-2. Structure of Syrian hamster PrP^{C} amino acids 125-228 from PDB 1B10 #4 [20], modified to include a representation of the intrinsically unstructured amino terminus (amino acids 23-124). Secondary structure is labeled by color (Red = α-helix, Blue = β-sheet, Grey = random coil and turns)

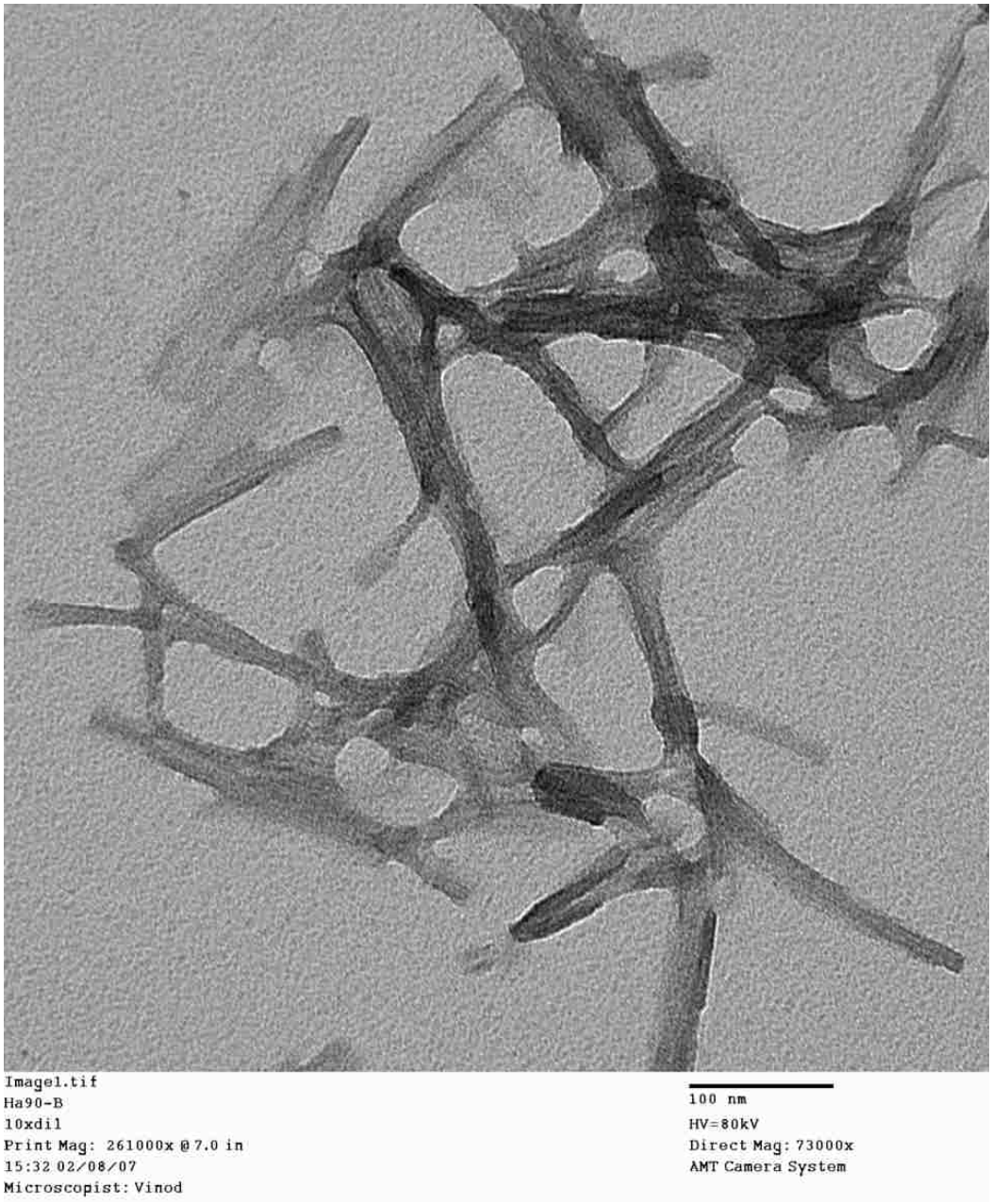

Figure 1-3. Electron micrograph of recombinant fibers made from Syrian hamster PrP 90-232 (PrP^{F}). Image was taken by the Rocky Mountain Laboratories Electron Microscopy facility under the direction of Dr. Roger Moore (Bar = 100 nm).

Although low resolution structural information of PrP^{Sc} has been

gathered and many models of possible structures have been generated (covered in detail in Chapter 5), crucial pieces of this puzzle are still missing. Determining the structure of the infectious protein unit remains one of the central mysteries in prion biochemistry. This is not only for academic reasons, such as the light it could shed on the protein-only hypothesis, but for practical reasons as well. Most importantly, this knowledge could allow for the rational design of both prophylactics to protect against initial infection, and treatments to halt or reverse the neurodegeneration and certain death associated with prion diseases. But even beyond the realm of prion disorders, because of the common protofilament nature of amyloid deposits, a structure of PrP^{Sc} could provide clues that lead to the prevention and treatment of all amyloid plaque diseases.

Through our research, we seek to elucidate structural differences between the recombinant PrP^{C}, β-oligomer, and PrP^{Sc} of truncated Syrian hamster PrP (residues 90 -232). We accomplished this task through the selective nitration of some of the ten tyrosine (Tyr) residues found in this domain and the determination of the modification sites using mass spectrometry. Specifically, we first sought to determine the reactivity of the Tyr residues in the recombinant soluble isoforms (PrP^{C} and the β-oligomer) of the prion protein using the nitrating reagents peroxynitrite (PN) and tetranitromethane (TNM). Next, we sought to determine the reactivity of the Tyr residues in the insoluble, recombinant fibrillar isoform

(PrP^F) of the prion protein with PN.

The rationale behind monitoring conformational changes through the nitration of tyrosine residues is basically three-fold (expanded upon in Chapter 6). First, nitration with PN and TNM is largely tyrosine-specific. Next, nitration is dependent on the degree to which each tyrosine residue is solvent exposed. Finally, Cashman and colleagues have detected an increase in tyrosine solvent exposure and the emergence of a Tyr-Tyr-Arg specific epitope upon PrP^C conversion to PrP^{Sc} [25]. Therefore, we hypothesize that structural differences among the three prion protein isoforms will be detectable by the selective nitration of tyrosine residues by PN and/or TNM. Furthermore, we hypothesize that more of the 10 Tyr residues present will become nitrated upon conversion from PrP^C to the β-oligomer or PrP^{Sc}. By detecting these differences in nitration patterns, we seek to provide crucial information about the structural differences that take place as the innocuous PrP^C converts to forms that resemble infectious PrP^{Sc}.

CHAPTER 2

MATERIALS AND METHODS

The overall experimental design is summarized as follows:

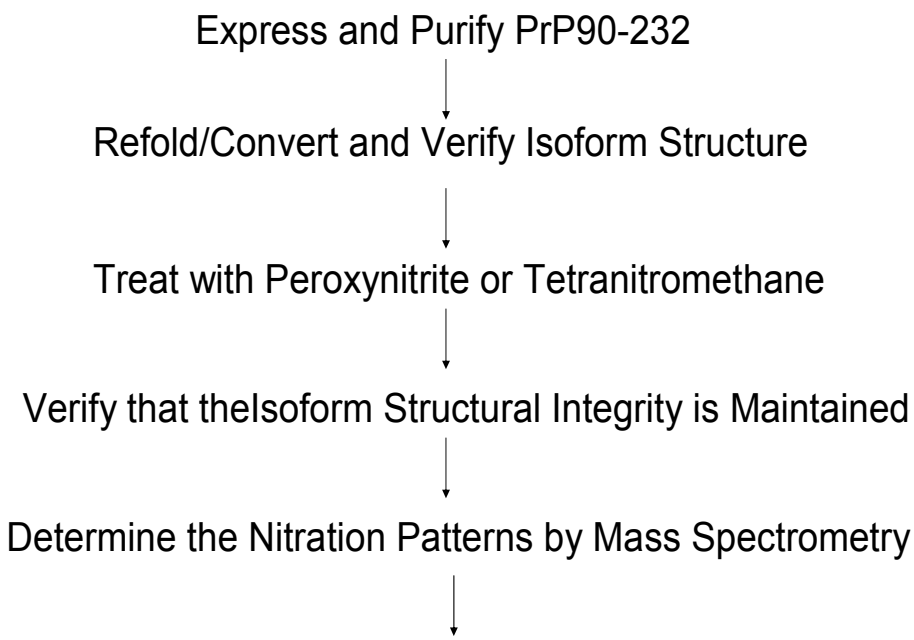

Express and Purify PrP90-232 WT: The gene encoding truncated WT Syrian Hamster PrP (residues 90-232, PrP90) was subcloned from the pHaPrP plasmid [24] into the pET24a^{+} vector. The resulting new plasmid, pET24PrP90, was transformed into *E. coli* BL21(DE3)-Rosetta cells (Novagen, Inc.). The expressed protein did not contain most of the unstructured amino-terminus, the GPI anchor, and was unglycosylated. This work was performed by Sam J. Chelmo.

The antibiotics kanamycin (50 µg/mL) and chloramphenicol (34

μg/mL) were added to select for transformed cells which were grown in liquid culture at 37°C in 2xYT media. Growth was measured by optical density at 600nm (OD_{600}) and cell cultures were grown until the OD_{600} reached 1.0. At this point, the lactose analog isopropyl-β-D-thiogalactoside (IPTG) was added in order to induce expression. For each liter of culture, 1 mL of 0.5M IPTG solution was added (to a final concentration 0.5 mM). Expression levels were typically above 15 mg/L. Following induction, cells were grown for 4 h, centrifuged, and frozen at -20°C overnight.

PrP90 was purified using modifications to a published procedure [26]. This process began with lysis of the frozen cells by resuspension in 50 mM TrisHCl at pH 7.5 with 100 μg/mL lysozyme and 10 μg/mL DNase I (lysis buffer). For every liter of cell culture originally grown, 50 mL of lysis buffer was used. The suspension was shaken at 37°C until the consistency was homogenous (~1.5 h) and the solution was then centrifuged.

PrP90 is expressed as inclusion bodies. To purify the inclusion bodies, the lysed cell pellet was resuspended in 50 mM TrisCl at pH 7.5 with 1% Triton X-100. After resuspension, the homogenate was placed on ice for 20 min., and then centrifuged. This step was repeated 3-5 times until the resulting pellet was a consistent white color.

Purified inclusion bodies were solubilized in buffer A (8 M urea, 0.1 M KPO_4, pH 8.0 with100 μg/mL protease inhibitor cocktail from Sigma).

The solution was once again centrifuged but in this case, the supernatant contained PrP90. This supernatant was then mixed with a Ni(II)-Chelating Sepharose resin (GE Healthcare) for 30 min. at room temperature to bind the PrP90. For every liter of cell culture, 50 mL of resin was used. The mixture of resin and PrP90 in buffer A was poured into a 5 cm diameter column and washed with buffer A. Periodically, the absorbance at 280 nm of effluent from the wash was measured and once the absorbance dropped below 0.03, the washing was stopped. Next, a 1 L linear gradient was set up to run from 100% buffer A to 100% buffer B (0.1 M KPO_4, pH 8.0), which served to refold the PrP on the column. After completion of the gradient, the column was washed with 100 mL of buffer B. Following this, the refolded PrP90 (PrP^C) was eluted from the column using buffer B containing 60 mM imidazole.

If contaminating proteins were present, samples were subjected to further purification using hydrophobic interaction chromatography (HIC) using a HiPrep Phenyl Sepharose 16/10 column (GE Healthcare). Protein was loaded onto the column in 6 M guanidine-HCl, 1 M NH_4SO_4, 10 mM KPO_4 at pH 8. To elute, a gradient from 1 M to 0 M NH_4SO_4 was run in the presence of 4 M urea, 25 mM TrisCl at pH 8.0.

Purity, as well as possible protease digestion of PrP90 during purification, were assessed after elution from the Ni(II)-chelating Sepharose column by SDS/PAGE (and again if the HIC step was necessary). Samples were mixed with TrisHCl pH 8 buffer containing

SDS and the reducing agent dithiothreitol (DTT) and boiled at 95°C for 5 min. Following this treatment, samples were run on 8-25% polyacrylamide gels using the Pharmacia PhastSystem (GE Healthcare). Coomassie blue staining was also completed using the Pharmacia PhastSystem. The BioRad broad range standards were used for mass determination. As determined by SDS/PAGE, the purity level of protein used for all nitration experiments was very high (figure 2-1.)

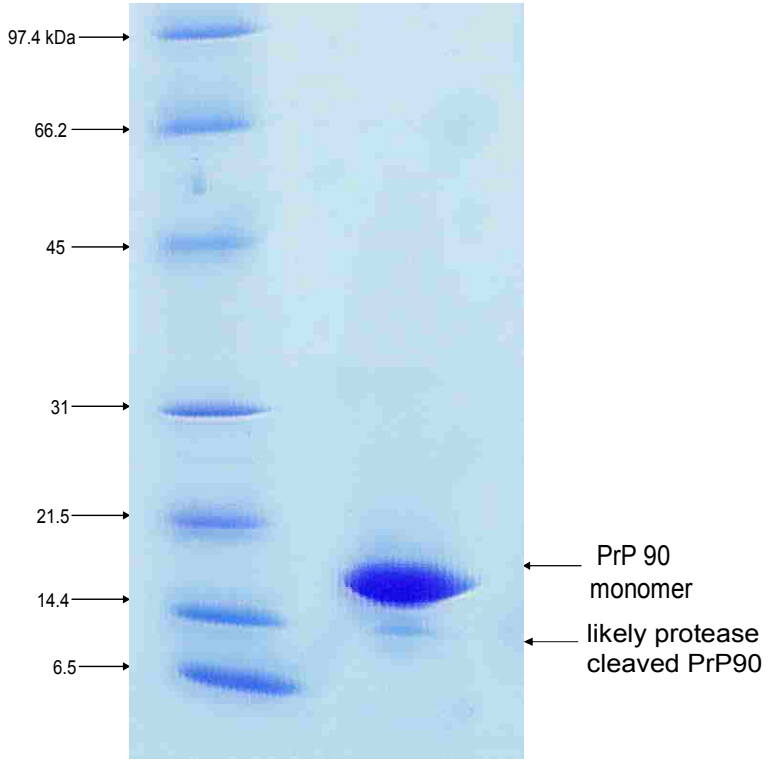

Figure 2-1. SDS/PAGE gel displaying the typical purity level of protein used for reaction.

Refold/Convert and Verify Isoform Structure: Purified PrP90 was either refolded to PrP^{C} or converted to the β-oligomer or to the fibrillar

form. To form PrP^C, the PrP90 was dialyzed into 10 mM ammonium acetate (NH_4OAc) buffer at pH 5.5.

The β-oligomer was formed by the dilution of 120 μM protein (initially in 6 M guanidine-HCl, 10 mM KPO_4 at pH 8) to 20 μM with conversion buffer (3.6 M urea, 160 mM NaCl, 60 mM NaOAc, pH 3.7) and incubation overnight at 37°C. Following incubation, the β-oligomer was dialyzed into 10 mM NH_4OAc at pH 5.5.

Recombinant fibrils (PrP^F) used were made by Dr. Roger Moore from the laboratory of Dr. Sue Priola at Rocky Mountain Laboratories by modifying a published procedure [13]. The PrP^F was analyzed at RML using electron microscopy and Fourier transform infrared spectroscopy (FT-IR). PrP^F used in these experiments was provided by Mr. Xu Qi and Dr. Scott Hennelly.

Before and after reaction with PN or TNM, the conformation of PrP^C or the β-oligomer was verified by circular dichroism (CD) spectroscopy using a Jasco 810 spectrophotometer and Asymmetric Flow Field Flow Fractionation (AF_4) using a Focus AF2000 with an in-line UV-visible electronic absorbance detector (PostNova, Inc.). CD is a technique that distinguishes secondary structural characteristics and AF_4 is a technique that resolves particles into distinct peaks based on shape and mass.

The β-sheet and α-helix have distinct CD spectroscopic signatures [27, 28]. In the case of β-sheet secondary structure, a single minimum is observed at about 214 nm. As for α-helix secondary structure, two

pronounced minima are observed at 222 nm and 209 nm.

When conducting an AF_4 run, at least 400 pmol of sample were injected and a 25 mM NaOAc, 3 M urea buffer at pH 5.0 was used throughout the procedure. The focusing step took place on a 4 kDa molecular weight cut off polyethersulfone membrane for 35 sec with crossflow of 3 mL/min and a channel flow 1 mL/min. The peak resolution step used a crossflow of 2 mL/min and a channel flow 1 mL/min.

Prior to nitration, PrP^C and β-oligomer protein concentration was determined by measuring the absorbance at 280 nm using an HP 8453A photodiode array spectrophotometer, and the calculated extinction coefficient of 26,025 M^{-1} cm^{-1} [29]. The Bio-Rad protein dye assay was used after nitration due to the interference of nitrotyrosine absorbance (figure 2-2). A protein standard curve was established vs. bovine serum albumin (BSA) using unlabeled PrP, from which a correction factor of 0.93 was calculated. Following this, BSA was used as the standard reference to determine PrP concentration. The structures of tyrosine and nitrotyrosine are shown in figure 2-3.

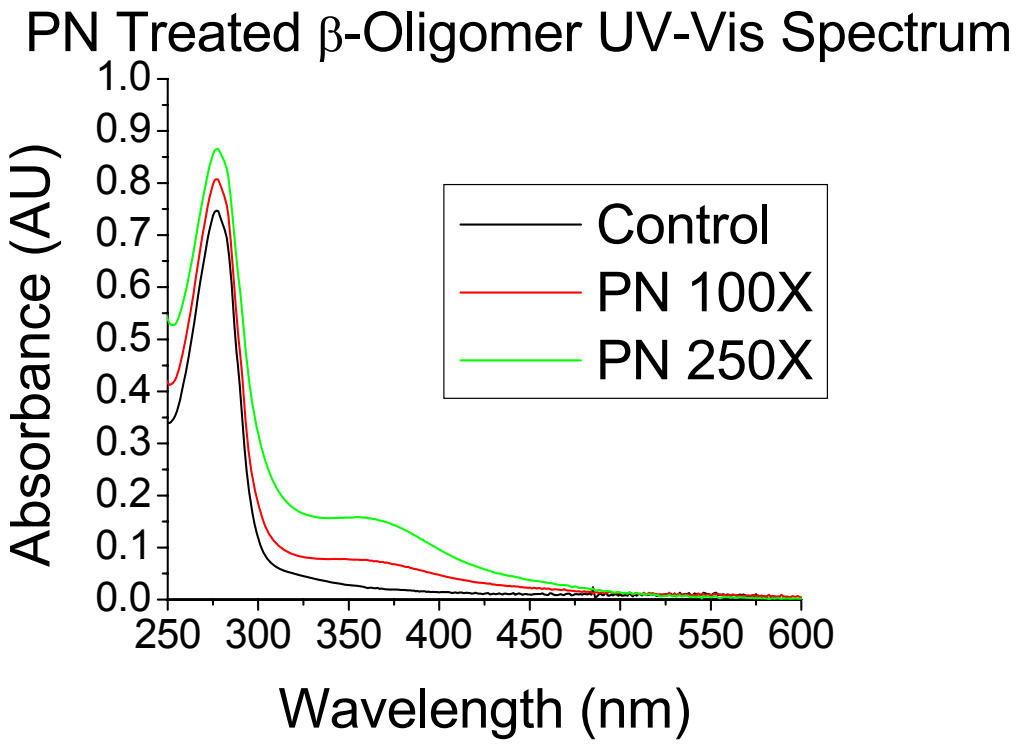

Figure 2-2. UV-visible electronic absorbance spectra showing an increase in absorbance at 280 nm and 360 nm of tyrosine residues upon nitration. Measurements were taken in 10 mM NH_4OAc, pH 5.5 and normalized to the concentration of the unmodified PrP90 sample at 27 μM.

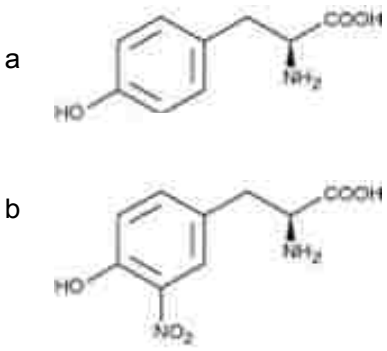

Figure 2-3. The structures of tyrosine (a) and nitrotyrosine (b).

The concentration of PrP^F was determined after denaturation in 6 M guanidine-HCl, 10 mM KPO_4 at pH 8 using the method of Pace et al [29]. PrP^F concentration was not determined following nitration because CD and AF_4 could not be performed. Instead, the samples were used "as is" for further work.

The percentage of common secondary structure motifs was determined for PrP^C and the β-oligomer by deconvolution of their CD spectra. Measurements were taken from 185-240 nm at 20°C and 25 scans were averaged. Cuvettes of 0.1 or 0.2 mm path length and protein concentrations from 7-14 μM of each isoform were used. Employing reference set #3 of the CDSSTR program of the online DICHROWEB server [27, 28], the percentages of secondary structures were calculated. Reference sets are groups of proteins with known structures and CD spectra used by DICHROWEB during deconvolution. Reference set #3 was used because it gave the result most consistent with the known secondary structure of Syrian hamster PrP^C [20].

For PrP^C, solvent exposure and secondary structure levels were assessed using MOLMOL software [30]. An average of the 25 best NMR solution structures (PDB 1B10, reference 20) of recombinant Syrian hamster PrP^C was used in calculations.

The thermal denaturation of untreated, 100-fold peroxynitrite, and 1000-fold treated PrP^C was measured using CD spectroscopy. Spectra

were taken in the range of 190-300 nm at 2°C intervals from 25-85°C.

Treat with Peroxynitrite or Tetranitromethane: The nitrating reagents peroxynitrite (PN) and tetranitromethane (TNM) were used to label reactive Tyr residues in the different PrP isoforms. PN was synthesized following a published procedure [31]. In this procedure, 20 mL of 0.6 M $NaNO_2$, 0.9 M H_2O_2 was added to 10 mL HCl. Five to six seconds later, 10 mL of 1.2 M KOH, and 400 μM diethylenetriaminepentaacetic acid (DTPA) was added. To improve the yield of potassium peroxynitrite, Dr. Scott Hennelly operated a SFM400 Biologic four-syringe quench flow system to mix the reagents (kindly provided by Dr. Walt Hill). Typical concentrations of potassium peroxynitrite obtained were 120 mM. After generation, the PN was stored at -70°C. TNM was purchased from Sigma-Aldrich and stored at -70°C. Special precautions were followed when using TNM (detailed below) due to its extreme toxicity. Both PN and TNM were used in this study because each reagent follows a different reaction mechanism (described in detail in Chapter 6) and thus their reactivites can be influenced by different factors.

To check the concentration of PN, the reagent was first diluted 100-fold in 1 M KOH and the UV-visible electronic absorbance spectrum was measured. The PN concentration was checked periodically by measuring the absorbance at 302 nm (extinction coefficient of 1670 M^{-1} cm^{-1}) and no detectable reduction in concentration occurred, even after 6 months.

Several concentrations of each reagent were tested to ensure effective nitration without secondary structure disruption and or significant amounts of cross-linking, which is a side reaction of tyrosine nitration. Mass spectrometry was performed on PrP^C after treatment with 100-fold PN, 150-fold PN, 250-fold PN, 100-fold TNM and 1000-fold TNM. For the β-oligomer, samples treated with 100-fold and 250-fold excess of each reagent were also analyzed by mass spectrometry. In the case of the PrP^F, samples reacted with 100-fold excess of PN were analyzed by mass spectrometry.

All reactions were done in at least triplicate. The PrP90 soluble isoforms were reacted at ~12 μM monomer protein concentration at pH 5.5 (the β-oligomer is unstable above pH 5.5). Treatments with PN used 200 mM 10 mM NH_4OAc, 10 μM DTPA, pH 5.5. Samples were allowed to react with PN for five minutes at room temperature.

The PrP^F PN reaction buffer was 150 mM NH_4OAc, 50 mM NH_4HCO_3 at either pH 5.5 or pH 7.5 (3 reactions done at each pH). Prior to reaction, the insoluble fibers were resuspended into a homogenous solution at a final concentration of ~120 μM. As an added precaution, reactions were performed under a biosafety laminar flow hood.

In the case of TNM, 50 mM NH_4OAc, pH 5.5 buffer was used. PrP^C was reacted overnight while the β-oligomer was reacted for 2 hours at room temperature. TNM was not reacted with PrP^F due to time constraints. Anaerobic conditions were employed during the TNM

treatments and reactions took place under a standard chemical fume hood.

Reactions intended to induce covalent cross-links were conducted in the same buffer as nitration reactions. The excess of PN or TNM used ranged from 250-fold to 1000-fold.

Following reaction of PrP^C or the β-oligomer with PN or TNM, byproducts were removed by dialyzing the samples into 10 mM NH_4OAc, pH 5.5. After PN reaction, PrP^F was centrifuged and the pellet collected. The sample was then denatured by resuspension in 8 M urea, 0.1 M KPO_4, pH 8.0 overnight at room temperature.

Verify Isoform Structural Integrity Maintained: Following PN or TNM treatment and purification from reagents via dialysis, the soluble isoforms were analyzed a second time by CD and AF_4. In the case of PrP^F, the conformation was verified at RML using electron microscopy prior to denaturation. These measurements were conducted to ensure that no gross structural changes occurred as a result of the reaction.

Mass Spectrometry: In preparation for mass spectrometry, a 10% trichloroacetic acid (TCA) precipitation was used to concentrate the PrP^C or the β-oligomer nitrated samples. In the case of PrP^F, 30% TCA was used following a 20-fold dilution of the denatured PrP^F (the urea concentration must be lowered for TCA precipitation to be successful).

Protein pellets were washed with 1:1 ethanol:ether solution before being re-suspended in 50 mM NH_4HCO_3 buffer at pH 8 and digested with trypsin (1:7.5 trypsin to protein ratio suggested by Dr. Holly Cox). Tryptic peptides expected are shown in table 2-1. Samples were digested overnight at 37°C, reduced with DTT for one hour at 56°C and finally dried under vacuum. Following this, samples were suspended in 80% ethanol and dried under vacuum again.

Tryptic Peptides of PrP90

Tyrosine-Containing?	Mass (Da)	Residues	Peptide Sequence
P4 (Y169)	**2475**	**165-185**	**PVDQYNNQNNFVHDCVNITIK**
P1 (Y128)	**2363**	**111-136**	**HMAGAAAAGAVVGGLGGYMLG SAMSR**
Internal Standard (IS)	**1534**	**137-148**	**PMMHFGNDWEDR**
P5 (Y218)	**1457**	**209-220**	**VVEQMCTTQYQK**
No	1283	90-101	GQGGGTHNQWNK
No	1153	195-204	GENFTETDIK
P3 (Y157, Y162, Y163)	**1102**	**157-164**	**YPNQVYYR**
P6 (Y225, Y226)	**1088**	**221-229**	**ESQAYYDGR**
No	1016	186-194	QHTVTTTTK
No	663	152-156	ENMNR
No	548	205-208	IMER
P2 (Y149, Y150)	**501**	**149-151**	**YYR**
No	493	107-110	TNMK
No	331	102-104	PSK
No	244	105-106	PK
No	193	230-231	SS
No	175	232	R

Table 2-1. Peptides generated from PrP90 digest with trypsin ordered by decreasing mass. Peptides containing tyrosine residues (P1-P6) are in bold, as well as the peptide used as an internal standard (IS). This table was generated using the PeptideCutter program[32].

Reduced peptides were re-suspended in 50% acetonitrile, 0.1% trifluoroacetic acid and mixed in equal parts with the matrix α-cyano-4-

hydroxycinnamic acid (CHCA) containing Bruker peptide standards I (table 2-2). Peptides were analyzed by Matrix Assisted Laser Desorption Ionization-Time of Flight mass spectrometry (MALDI-TOF MS) using the Applied Biosystems Voyager MALDI-TOF mass spectrometer. All mass spectrometry was performed at the University of Montana Mass Spectrometry and Proteomics Core Facility). Dr. Holly Cox performed most of the MALDI-TOF mass spectrometry on the PrP^C and the β-oligomer isoforms.

Protein Standard	Mass (Da)
ACT clip 18-39	2465
ACT clip 1-27	2093
Bombesin	1619
Substance P	1347
Angiotensin I	1296
Angiotensin II	1046

Table 2-2. External protein standards used for calibration during MALDI-TOF MS (Bruker).

To assess the efficiency of the tryptic digests, a number of different factors were analyzed. MALDI-TOF MS showed that most of the signal arose from fragments smaller than 3000 amu, and there were no peaks in the range of undigested PrP. Furthermore, between the range of 450-5000 amu, well over 90% of the predicted tryptic peptides were identified.

In most samples, no missed cleavages were seen, even in the case where trypsin is less likely to cleave (when proline immediately follows lysine or arginine).

The peptide composed of amino acids 209-220 containing Y218 was difficult to detect using MALDI-TOF MS. Therefore, a greater range of error should be assumed for this peptide.

Prior to assessing the degree of nitration, raw spectra were modified using the Data Explorer program (Applied Biosciences). Employing the basic options of Data Explorer, the data were baseline corrected, noise-filter smoothed, de-isotoped, and mass calibrated using the Bruker standards.

The level of nitration for each Tyr-containing peptide was determined as the percentage of all the nitrated species of a peptide compared with all identified forms of the peptide. MALDI-TOF MS often results in the loss of one or two oxygen atoms from the nitrotyrosine group via photodecomposition [33]. Thus, the peak intensities of the un-nitrated peptide, nitro peptide, nitro – 1 oxygen peptide, nitro – 2 oxygen peptide, as well as possible methionine oxidized peptides were determined. (If methionine is present, oxidation can occur, which adds an additional oxygen to the peptide mass.) Once all forms of a peptide were identified (see Appendix), the areas of the peaks derived from nitrated tyrosine species were summed and then divided by the sum of all the peak intensities.

For this method of determining the level of nitration to be valid, nitrotyrosine containing peptides must desorb from the matrix in the same way as the corresponding unmodified and methionine-oxidized peptides. To determine if this was true, a non-tyrosine containing prion peptide (amino acids 137-148) was used as an internal standard. The total peak intensity for each tyrosine-containing peptide, both in nitrated and unnitrated samples, was compared with the intensity of the internal standard. This analysis showed that there was no nitration-dependent trends in matrix desorption.

Sequencing Electrospray Tandem Mass Spectrometry: To confirm the site(s) of nitration on tryptic peptides containing more than one tyrosine, sequence information was obtained by electrospray ionization (ESI) tandem mass spectrometry (MS/MS) analysis using a QTOF micro (Waters, Milford, MA). As the tryptic YYR peptide (residues 149-151) was too small for ESI analysis, a cyanogen bromide digestion (table 2-3) was performed instead. TCA precipitated protein pellets (15 μg) were mixed with CNBr in 70% TFA at room temperature for 24 hours. The digestion solution was removed under vacuum. Peptides from both trypsin and cyanogen bromide digestion were resuspended in 2% acetonitrile, 0.1% formic acid and separated by capillary liquid chromatography using a CapLC XE (Waters) coupled to the ESI source of the QTOF micro. The peptides were concentrated and desalted with an in-line C_{18} PepMap™

Nano-Precolumn, 5 mm x 300 μm, 5 μm particle size (Dionex) followed by reversed phase separation on a Waters C_{18} capillary column (15 cm x 75 μm i.d., 3 μm particle size). Peptides were eluted from the column with a 70-minute linear gradient of acetonitrile from 10-40% in 0.1% formic acid. The voltages were set at 3800 V for the capillary, 38 V for the sample cone and 3.0 V for the extraction cone. Mass spectra were acquired between the range of 200-1500 m/z followed by data-dependent selection of ions for MS/MS. To enhance the selection of low abundance nitropeptides for MS/MS, only ions with m/z values that corresponded to nitropeptide masses with a 2+ or 3+ charge state were selected for collision induced dissociation fragmentation. Ions with m/z values corresponding to the unmodified peptides were not selected for MS/MS. Collision voltages were dependent upon the m/z and charge state of the parent ion. MS/MS spectra were analyzed using Mascot Daemon (Matrix Science) to search a database containing the hamster PrP90 sequence. Methionine oxidation and nitrotyrosine were selected as variable modifications. Mass accuracy was set to 50 ppm for peptide tolerance and 0.2 Da for MS/MS tolerance. All ESI-MS/MS and CNBr digests were performed by Dr. Holly Cox.

CNBr Peptides

Mass (Da)	Residues	Peptide Sequence
6156	155-206	NRYPNQVYYRPVDQYNNQNN FVHDCVNITIKQHTVTTTTKGENFTET DIKIM
2271	214-232	CTTQYQKESQAYYDGRRSS
2119	90-109	GQGGGTHNQWNKPSKPKTNM
1983 (P2b)	**140-154**	**HFGNDWEDRYYRENM**
1344	113-129	AGAAAAGAVVGGLGGYM
842	207-213	ERVVEQM
442	135-138	SRPM
430	130-134	LGSAM
367	110-112	KHM
102	139	M

Table 2-3. Peptides generated from PrP90 digest with CNBr ordered by decreasing mass. P2b contains tyrosines 149 and 150.

CHAPTER 3: PrP^C

Adapted from Lennon et al., *Biochemistry,* **46**, 4850-60, 2007.

Introduction

PrP^C is a soluble monomer dominated by three α-helices, with two short β-strands (see figure 1-2). PrP^C contains a long intrinsically unstructured amino-terminal domain comprised of amino acids 23 to ~108. The protein normally resides on the external surface of cells, is mainly neuronal, and contains a transitory signal peptide (amino acids 1-22) that directs its delivery. It is attached to the plasma membrane by a glycosylphoshatidylinositol (GPI) anchor, coded by amino acids 233-254 which are removed as part of the GPI processing [34].

Remarkably, the function of PrP^C is not yet known. Further adding to the mysterious nature of this highly conserved and abundant (in some tissues) protein is that knockout mice not expressing any PrP^C appear to develop and behave normally [5], although their susceptibility to oxidative stress may be higher than wild type mice [35].

Some basic facts are known about PrP^C that are likely related to function, two of which are best supported. First, the intrinsically unstructured amino- terminus has the ability to bind copper (II) and thus may serve some role in copper homeostasis [35]. Second, PrP^C has some protective function against oxidative stress and may serve to protect the cell in that capacity [35].

Certain variations, germline and spontaneous mutations in the PrP^C

gene can lead to the formation of PrP^{Sc} and eventual death [36]. Germline and sporadic mutations are also involved in the formation of other amyloid diseases as well [37]. The most common human prion allelic variation is at residue 129, which can be a methionine or valine. The presence of valine at 129 appears to accelerate the misfolding of PrP^{C} [38]. To review some of the most frequent germline or sporadic mutations that result in disease, we will consider three of these prion diseases; Fatal Familial Insomnia (FFI), Creutzfeldt-Jakob disease (CJD) and Gerstmann-Sträussler-Scheinker syndrome (GSS). When D178 is mutated to an asparagine residue, FFI results [39]. If the M129V allele is present along with the D178N mutation, then Creutzfeldt-Jakob disease develops. Finally, when proline 102 is mutated to leucine, then GSS results .

Materials and Methods

A detailed description of the materials and methods used is provided in Chapter 2. Briefly, PrP^{C} was treated with varying levels of peroxynitrite (PN) and tetranitromethane (TNM). Samples treated with 100-fold and 250-fold PN and TNM were analyzed by circular dichroism (CD) and asymmetric flow field flow fractionation (AF_4) to assess whether structural changes had occurred. Matrix Assisted Laser Desorption/Ionization mass spectrometry (MALDI-TOF MS) was performed on the 100-fold PN and TNM treated samples to determine the tryptic peptides that became nitrated. Sequencing of the peptides was

done using Electrospray Ionization tandem mass spectrometry (ESI/MS-MS) to determine which tyrosine residue was nitrated on peptides with multiple tyrosines. Samples treated with up to 100-fold or 250-fold PN were analyzed by SDS/PAGE to determine if any covalent cross-links between PrP monomers were present. CD deconvolution was performed to determine the secondary structure of PrP^C using the DICHROWEB online server. Solvent accessible surface area was performed using the MOLMOL program.

Results

PrP^C sensitivity to PN and TNM: PrP^C is more sensitive to treatment with PN than TNM. Analysis of the CD spectrum of PrP^C fits very well with the known structure and is consistent with previous measurements. CD analysis shows a loss in α-helical secondary structure with PN treatment above 100-fold, detected by a loss of negative signal at 222 nm (figure 3-1). The formation of covalently linked higher order aggregates is also observed with AF_4 as the increase in absorbance at higher retention times (figure 3-2) in PrP^C treated with PN.

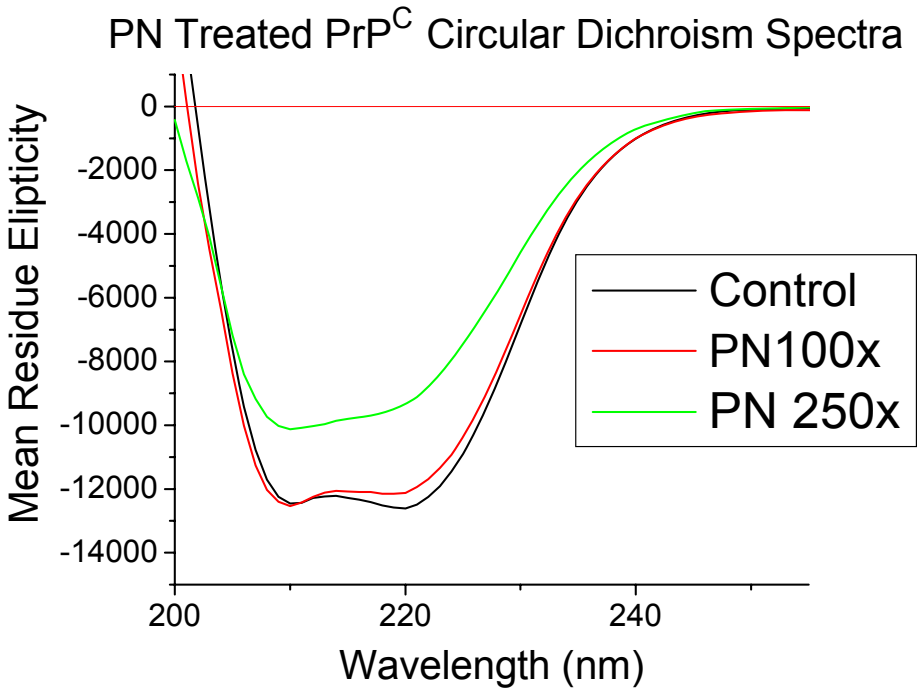

Figure 3-1. CD spectrum of PN treated PrP^C.

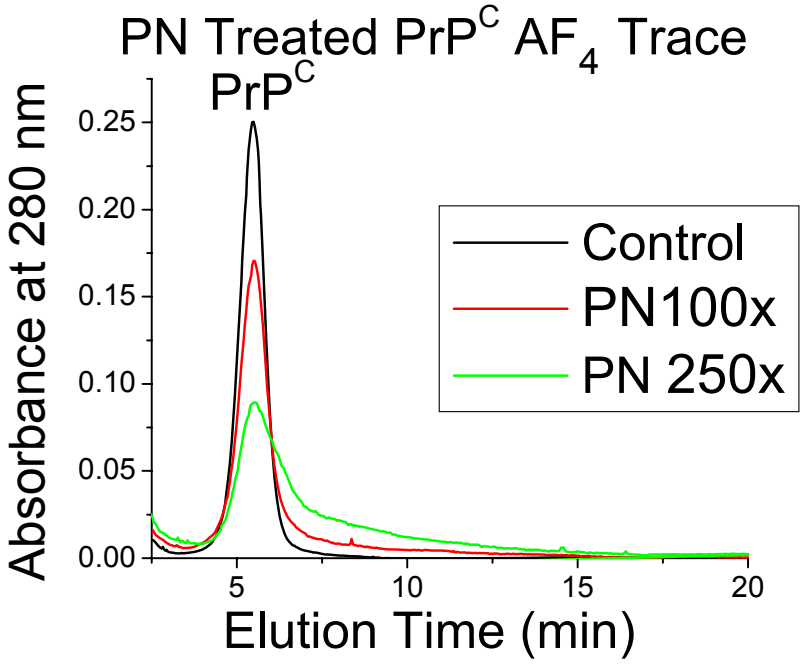

Figure 3-2. AF_4 trace of PN treated PrP^C.

In contrast, PrP^C treated with 1000-fold TNM maintains its secondary structure as measured by CD (figure 3-3). Furthermore, higher order aggregates are not observed by AF_4 (figure 3-4).

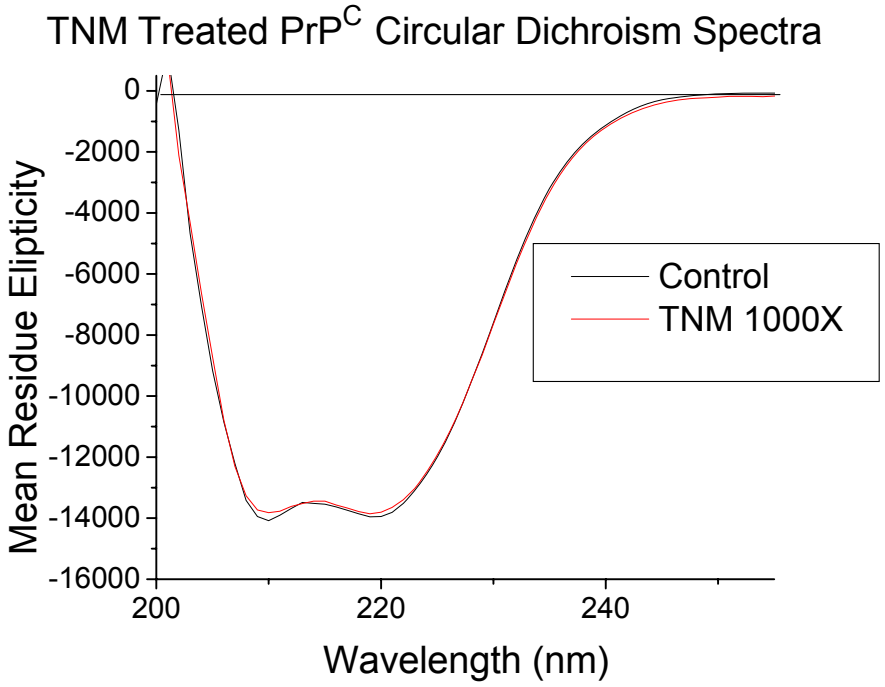

Figure 3-3. CD spectrum of TNM treated PrP^C.

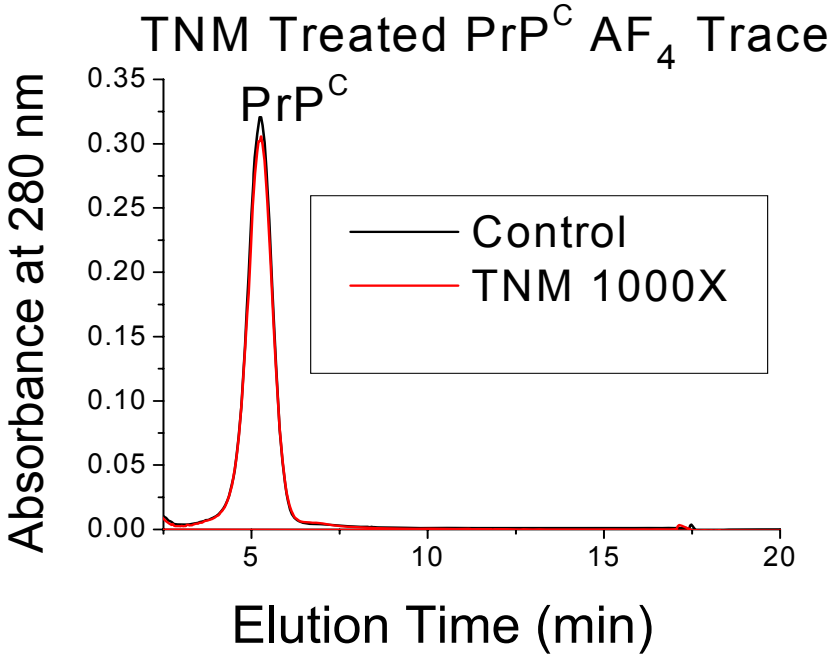

Figure 3-4. AF_4 trace of TNM treated PrP^C.

Covalent cross-linking: The AF_4 elution traces for 100 and 250-fold PN treated PrP^C show the formation of higher mass species (figure 3-2). In the case of TNM treated PrP^C, no higher mass species are observed, even with 1000-fold treatment (figure 3-4). To test whether these higher order aggregates were covalently cross-linked, SDS-PAGE was performed. The results show that these higher mass species detected after PN treatment are aggregates of covalently cross-linked, non-reducible PrP^C monomers (figure 3-5).

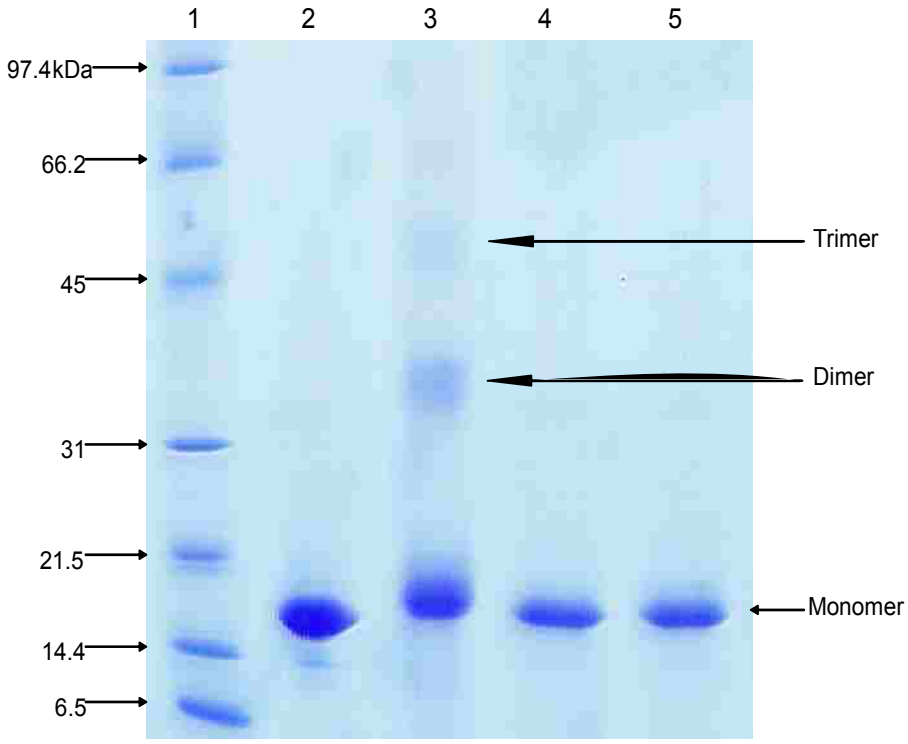

Figure 3-5. SDS/PAGE of PrP^C. Lanes: BioRad SDS broad range protein standard (1), Untreated PrP^C (2), 250X PN treated PrP^C (3), 250X TNM treated PrP^C (4), 1000X TNM treated PrP^C (5).

PrP^C nitration pattern with PN and TNM: PrP^C labeling patterns with 100-fold PN, 100-fold TNM and 1000-fold TNM are summarized in Table 3-1. The level of nitration reported is an average of three separate nitration experiments.

Tryptic Peptide Sequence		**100x PN PrP^C**	**100x TNM PrP^C**	**1000x TNM PrP^C**
P1 (residues 111-136) HMAGAAAAGAVVGGLGG**Y_{128}**MLGSAMSR		**+**	**-**	**-**
P2 (residues 149-151) **$Y_{149}Y_{150}$**R	Mono-nitration	**-**	**-**	**-**
	Di-nitration	**-**	**-**	**-**
P3 (residues 157-164) **Y_{157}**PNQV**$Y_{162}Y_{163}$**R	Mono-nitration	**+**	**-**	**+**
	Di-nitration	**-**	**-**	**-**
	Tri-nitration	**-**	**-**	**-**
P4 (residues 165-185) PVDQ**Y_{169}**NNQNNFVHDCVNITIK		**-**	**-**	**++**
P5 (residues 209-220) VVEQMCTTQ**Y_{218}**QK		**+++**	**-**	**+++**
P6 (residues 221-229) ESQA**$Y_{225}Y_{226}$**DGR	Mono-nitration	**++++**	**+**	**++++**
	Di-nitration	**++**	**-**	**++**

Table 3-1. MALDI/TOF analysis of Tyr-containing PrP peptides produced by trypsin digestion. Nitration Key: **-**, 0 to 5% nitration; **+**, 6 to 20% nitration; **++**, 21 to 45% nitration; **+++**, 46-70%, **++++**, 71 to 100% nitration.

The nitration pattern of PrP^C with 100-fold PN treatment (figure 3-6) includes Y128, mono-nitration at either Y162 or Y163 on the 157-164 peptide, Y218, Y225 and Y226. Highest labeling occurs at the carboxy-terminus of the protein, on the peptide containing Y225 and Y226. With 100-fold TNM treatment, little nitration was observed. Only a small amount of mono-nitration on the 221-229 peptide containing two tyrosines was detected. When PrP^C was subjected to 1000-fold TNM treatment, a

nitration pattern similar to 100-fold PN treatment was detected with two exceptions. The 100-fold PN treatment led to nitration at Tyr128, without nitration at Tyr169, while the 1000-fold TNM treatment led to nitration at Tyr169, without nitration at Tyr128.

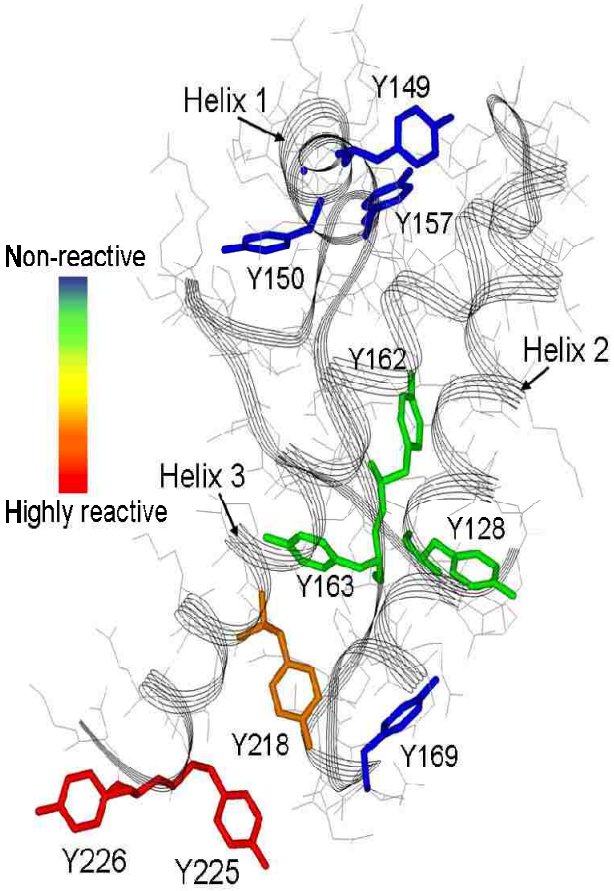

Figure 3-6. Structure of hamster PrP^C [20] indicating the locations and relative reactivities of the 10 Tyr residues after treatment with 100x PN.

A MALDI-TOF spectrum of peptides from the tryptic digest of PrP^C, after reaction with 100X PN (figure 3-7) as well as a portion of this spectrum enlarged to show the nitration levels of the 157-164 and 221-229

peptides (figure 3-8) is provided. The data for reaction with 1000X TNM are similarly reported in figures 3-9 and 3-9. A mass table showing all of the possible peptides of interest is provided in the appendix.

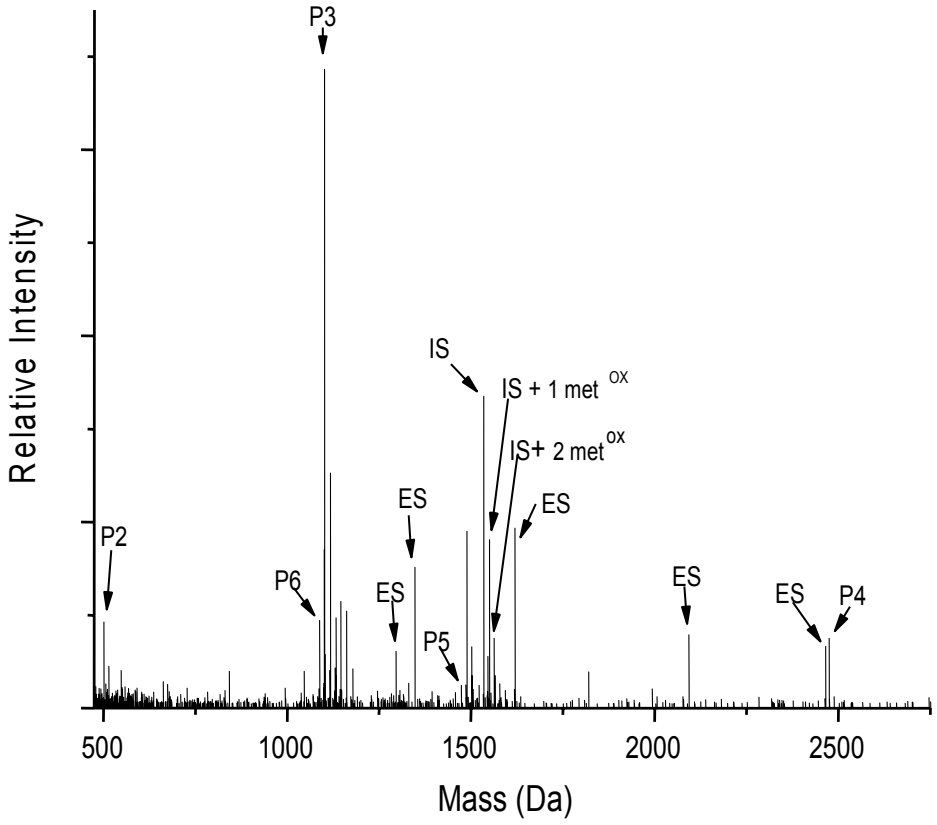

Figure 3-7. A partial MALDI-TOF spectrum of peptides from the tryptic digest of PrP^C, after reaction with 100x PN. P2-P6 = tyrosine containing tryptic peptides (P1 observed in different MALDI-TOF mode), IS = internal standard, ES = Bruker external protein standards (listed in table 2-2).

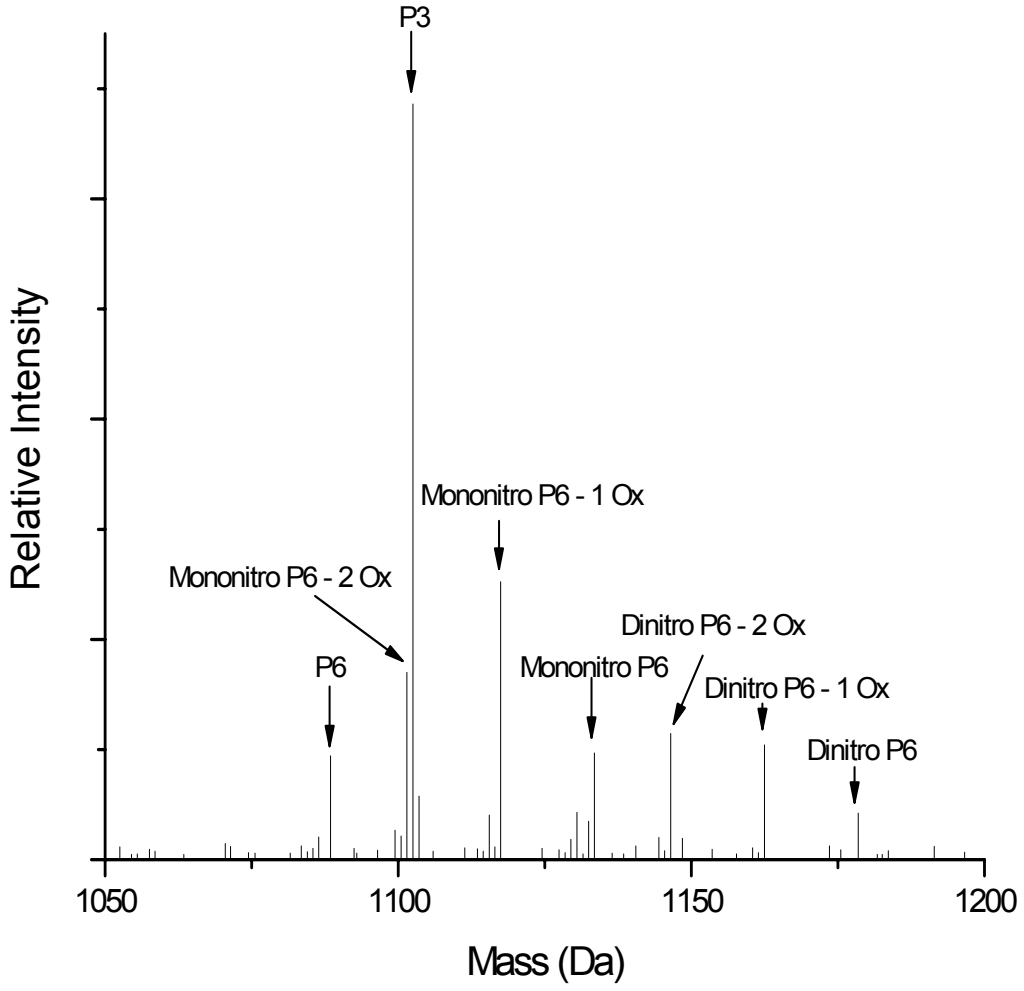

Figure 3-8. The partial MALDI-TOF spectrum in figure 3-7 showing the peptides observed from loss of one or both oxygens from the nitro-group as well as the levels of nitration for P3 and P6. P2-P6 = tyrosine containing tryptic peptides (P1 observed in different MALDI-TOF mode), IS = internal standard, ES = Bruker external protein standards (listed in table 2-2).

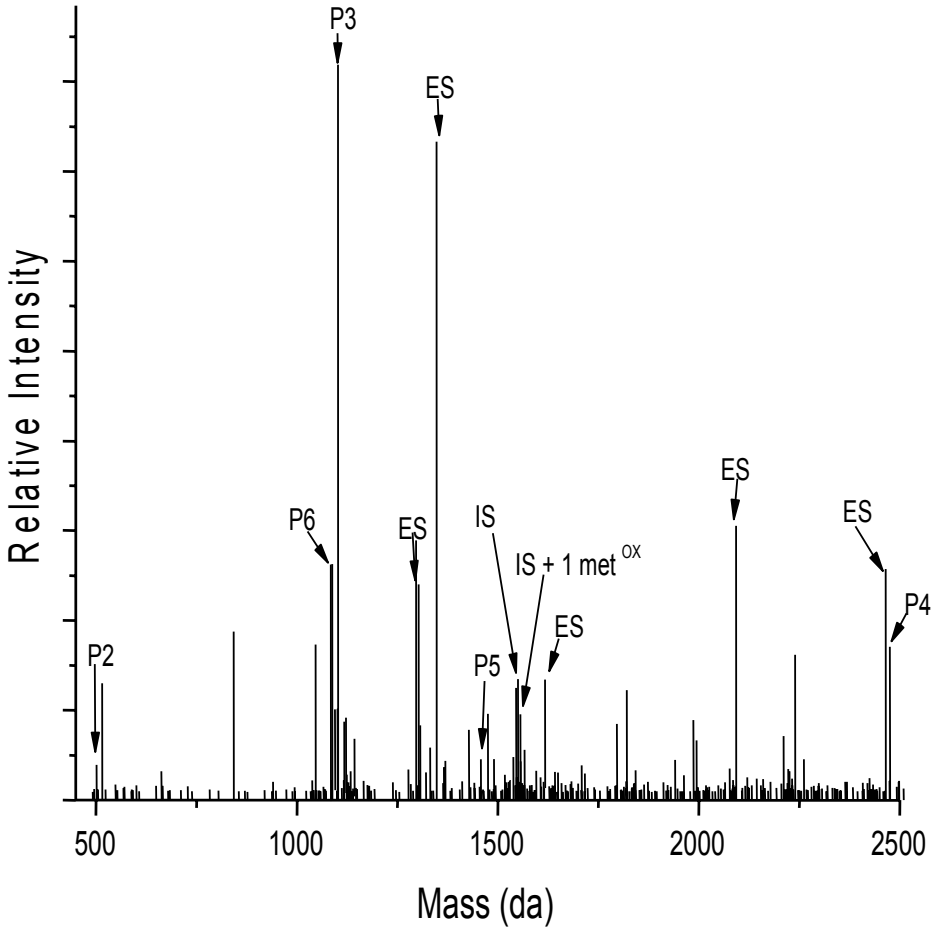

Figure 3-9. A partial MALDI-TOF spectrum of peptides from the tryptic digest of PrP^{C}, after reaction with 1000x TNM. P2-P6 = tyrosine containing tryptic peptides (P1 observed in different MALDI-TOF mode), IS = internal standard, ES = Bruker external protein standards (listed in table 2-2).

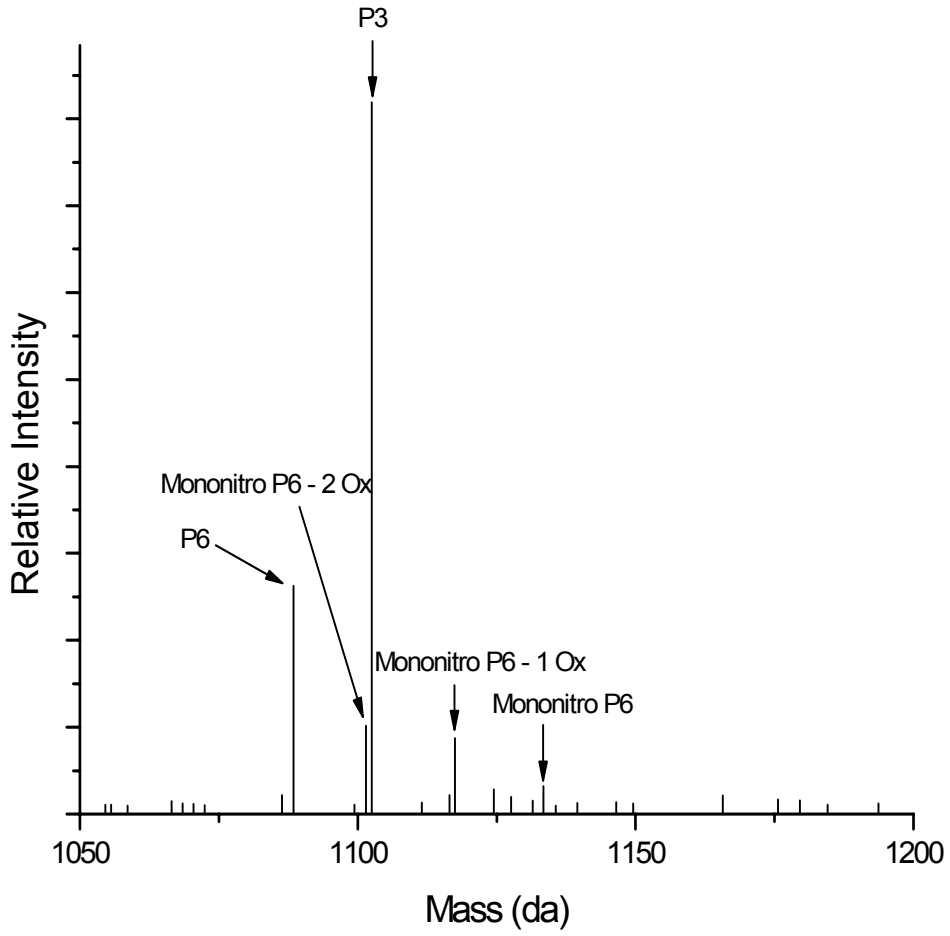

Figure 3-10. The partial MALDI-TOF spectrum in figure 3-9 showing the loss of one or both oxygens from the nitro-group as well as the levels of nitration for P3 and P6. P2-P6 = tyrosine containing tryptic peptides (P1 observed in different MALDI-TOF mode), IS = internal standard, ES = Bruker external protein standards (listed in table 2-2).

Electro Spray Ionization Tandem Mass Spectrometry: Protein sequencing using ESI/MS-MS was performed by Dr. Holly Cox for the

peptides containing more than one tyrosine. Sequencing results indicate that the 157-164 peptide could be labeled at Y162 or Y163, but no nitration was observed at Y157. For the 221-229 peptide, nitration was detected at both Y225 and Y226.

PrP^C Solvent accessibility predictions by MOLMOL: Solvent accessibility calculations were performed using MOLMOL software for the PrP^C Syrian hamster NMR structure PDB 1B10 [20], averaging the results of all NMR structures. The labeling patterns with 100-fold PN and 1000-fold TNM follows solvent accessibility predictions for most tyrosine residues, with exception to Y218. The results of these calculations are summarized in Table 3-2.

Tyrosine residue	128	149	150	157	162	163	169	218	225	226
Nitration Level 100X PN	+	-	-	-	+	+	-	+++	++++	++++
Nitration Level 1000X TNM	-	-	-	-	+	+	++	+++	++++	++++
Solvent accessible surface area (%)	5.6	13.7	2.8	2	11.7	3.3	16.4	5.6	39	59

Table 3-2: The Solvent Accessible Surface Area (SASA), as calculated using the MOLMOL program for the average value for all NMR solution structures from PDB #1B10 [20], is shown, along with the nitration levels

for each tyrosine residue.

Thermal Stability: The thermal stabilities of wild-type, 100-fold PN treated, and 1000-fold TNM treated PrP^C were determined using CD. While the untreated and 1000-fold TNM treated PrP^C displayed similar midpoint temperatures of unfolding of 68°C and near two-state behavior, the 100-fold PN- treated sample unfolded at 58°C and deviated significantly from two-state behavior (figure 3-11). As indicated earlier, the level and pattern of nitration were similar between the 100-fold PN and 1000-fold TNM treated samples, except in relation to Y128 and Y169. Also, some differences in the degree of methionine oxidation were observed between the two samples. These results showed a higher level of methionine oxidation in the PN treated sample.

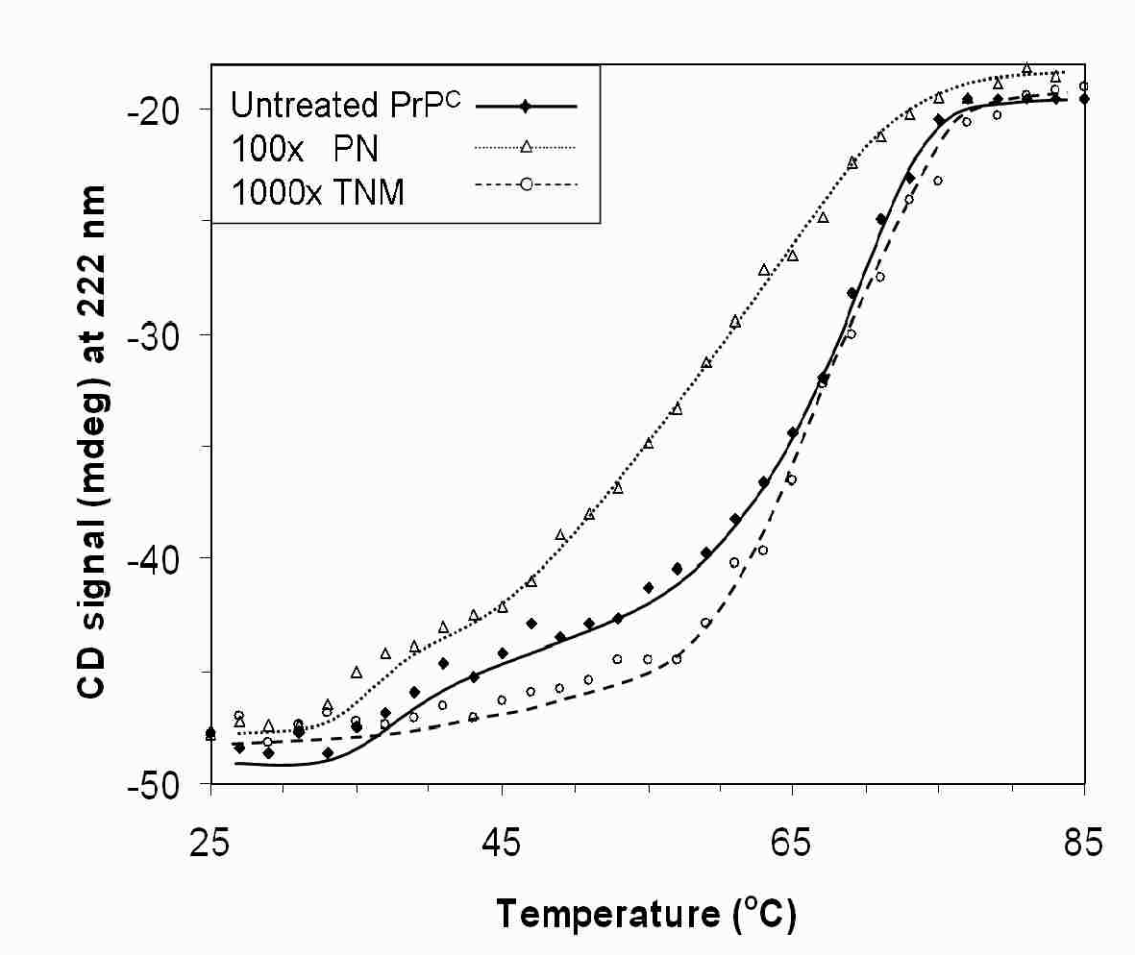

Figure 3-11. Thermal denaturation of PrP^c before and after treatment with 100x PN or 1000x TNM, as followed by the loss in CD signal at 222 nm (loss of α-helicity).

CD Deconvolution: The deconvolution of PrP^c was performed and the results are summarized in table 4-2. The amount of β-sheet secondary structure was overestimated when compared to the NMR structure, but otherwise the results were consistent.

Discussion

In the case of PrP^C, the availability of NMR structures provides a structural framework to interpret the nitration results. By examining the nitration patterns of PrP^C in comparison with structural analysis, we can draw conclusions about the factors influencing reactivity of the nitrating reagents (PN and TNM mechanistic details described in Chapter 6).

Solvent accessibility as calculated by MOLMOL for the 1B10 NMR structures of PrP^C do not follow nitration patterns exactly, and therefore should not be used to predict sites of nitration using PN or TNM. For example, MOLMOL predicts that Y225 and Y226 are most solvent accessible in PrP^C, which is consistent with our results. Therefore, with both PN and TNM, the most surface exposed residues in PrP^C (Y225 and Y226) are by far the most highly reactive. However, Y218 displays high levels of reactivity and MOLMOL predicts that this residue is virtually buried. One possible explanation for the reactivity of Y218 is that nitration of Y225 and/or Y226 leads to a conformational change of Y218, increasing its solvent accessibility.

When comparing the reactivity of PrP^C toward PN and TNM, an interesting result is found. PrP^C is much less reactive toward TNM than PN. Only low levels of mono-nitration are detected on the 221-230 peptide with 100-fold TNM in PrP^C. Strikingly, a 1000-fold molar excess of TNM is required to achieve a similar amount of nitration as detected with 100-fold PN. Initially, this result was not surprising due to the low pH of

the reactions, which does not favor TNM reactivity. However, as described in Chapter 4, 100-fold TNM nitrates the β-oligomer as efficiently as 100-fold PN. Therefore, it is likely that pH is not influencing the reactivity of TNM. The reason for this difference in TNM reactivity is unknown, although one possible explanation is that the PrP^C experiments were performed early on, when inaccuracies in technique are more likely to occur.

Unexpectedly, evidence has also been gathered suggesting that a single tyrosine residue may play an important role in the stability of PrP^C. One important difference in the nitration patterns of PrP^C with PN and TNM is noted at Y128. Low levels of nitration at this tyrosine are detected with 100-fold PN treatment, while no nitration at Y128 occurs even after 1000-fold TNM treatment. Temperature denaturation of wild type, 100-fold PN, or 1000-fold TNM treated PrP^C (figure 3-11) shows that the stability of 100-fold PN treated sample decreases considerably, while the 1000-fold TNM treated sample does not change compared with the untreated sample. Upon treatment of PrP^C with >150-fold PN, a considerable loss in α-helicity is measured by CD, which corresponds to an increase in nitration at Y128. Possibly, a subset of the sample representing the portion that is nitrated at Y128 unfoldd at lower temperatures, leading to an overall decrease in α-helicity.

This result is not surprising, considering the wealth of data gathered on the importance of methionine 129 in prion biology [38, 39]. M129 is

adjacent to Y128, which forms a hydrogen bond with aspartate 178. If nitration were to occur at Y128, it is possible that this could disrupt the Y128/D178 hydrogen bond, leading to a decrease in overall protein stability. It has been postulated that the D178N mutation in FFI destabilizes PrP^C for the same reason [40], further supporting this conclusion. However, this claim cannot be definitively made because a higher amount of methionine oxidation was also present in the PN-treated samples (data not shown), and it is possible that increased oxidation of the protein overall or at M129 caused the decrease in PrP^C stability.

Chemical cross-links are observed by SDS/PAGE at high PN concentrations. The CD spectra of these samples indicate that the protein monomer is largely unfolded under these conditions. Therefore, the cross-links are attributed to reactivity between Tyr residues of unfolded monomers, as dityrosine formation has previously been observed as a side reaction of nitration [41]. When the structure of PrP^C is maintained, cross-links between monomers do not form.

CHAPTER 4: β-Oligomer

Adapted from Lennon et al., *Biochemistry,* **46**, 4850-60, 2007.

Introduction

The β-oligomer is a soluble aggregated isoform (8-12 subunits) of PrP rich in β-sheet secondary structure [13, 42, 43]. β-oligomers may be formed from recombinant full length PrP lacking the GPI anchor [42], while in other cases, such as ours, recombinant truncated lacking the GPI anchor [13, 43]. The β-oligomer forms at low pH in denaturing conditions (see Chapter 2). Following our procedure (modified from reference 13 by Dr. Scott Hennelly), an octomer is formed (as determined by AF_4 by Dr. Scott Hennelly), which is consistent with previous studies [13, 43].

The β-oligomer shares secondary structural characteristics with PrP^{Sc}, most notably a large increase in the amount of β-sheet character upon conversion from PrP^{C} [13, 43]. It should be noted that although the β-oligomer is not believed to be on the kinetic pathway leading from PrP^{C} to PrP^{Sc} (i.e., not an intermediate) [13], it is however an aggregated form of PrP^{C} that is an intriguing model of PrP^{Sc} for a number of reasons. Beyond the mere secondary structure similarity, the β-oligomer has been shown to be toxic to neuronal cells [42], but is not infectious as with PrP^{Sc}. The β-oligomer has also been shown to assemble into fibrils upon prolonged incubation [43]. Furthermore, similarly sized particles (14-28 subunits) made from physical disruption and separation of PrP^{Sc} fibrils were found to be more infectious than the large fibrils, per protein subunit

[44].

As noted previously, detailed structures of PrP^{Sc} and the β-oligomer have not been solved. Therefore, it cannot be stated that the β-oligomer has a similar overall structure as PrP^{Sc}. However, we believe that the data suggest that the β-oligomer may represent an important model for studying the structure of PrP^{Sc} and, due to its superior tractability, is worthy of biophysical investigation.

Materials and Methods

A detailed description of the materials and methods used is provided in Chapter 2. Briefly, the β-oligomer was treated with varying levels of peroxynitrite (PN) and tetranitromethane (TNM). Samples treated with 100-fold and 250-fold PN and TNM were analyzed by circular dichroism (CD) and asymmetric flow field flow fractionation (AF_4) to assess whether structural changes had occurred. Matrix Assisted Laser Desorption/Ionization Mass Spectrometry (MALDI-TOF MS) was performed on 100-fold PN and TNM treated samples to determine which tryptic peptides became nitrated. Sequencing of the peptides was done using Electrospray Ionization tandem mass spectrometry (ESI/MS-MS) to determine which tyrosine residue was nitrated on peptides with multiple tyrosines. Samples treated with up to 100-fold or 250-fold PN were analyzed by SDS/PAGE to determine if any covalent cross-links between PrP monomers were present. CD deconvolution was performed to

determine the secondary structure of the β-oligomer using the DICHROWEB online server.

Results

The β–oligomer does not show varying sensitivity levels to PN and TNM: The β-oligomer does not display differing levels of sensitivity to treatment with PN compared with TNM. Additionally, analysis of the CD spectra does not indicated any significant protein unfolding with PN (figure 4-1), although some higher order aggregates were observed in the AF_4 traces (figure 4-2. Similar results were obtained for TNM treatment at either 100-fold or 250-fold molar excess (figure 4-3, figure 4-4).

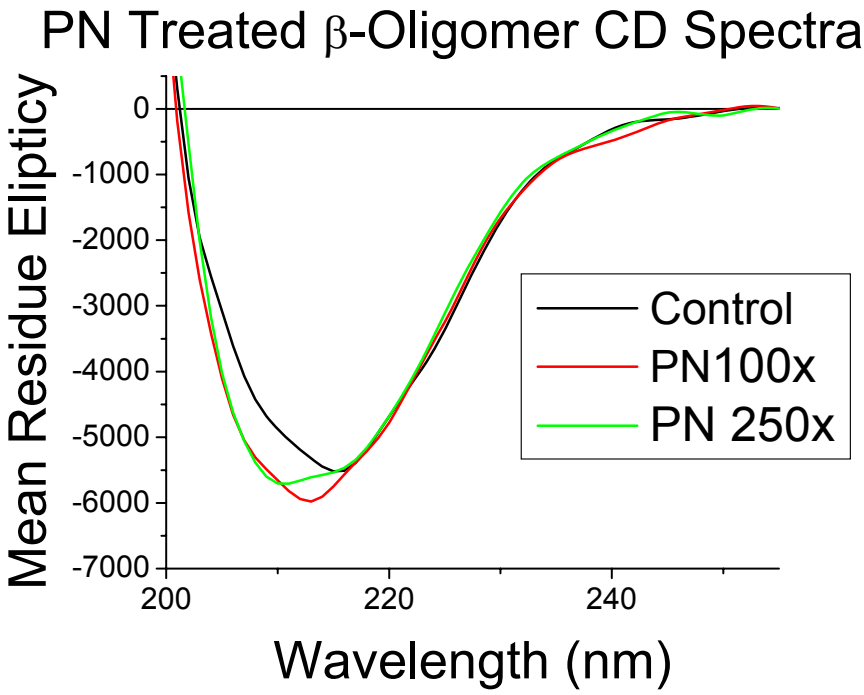

Figure 4-1. CD spectrum of PN treated β–oligomer.

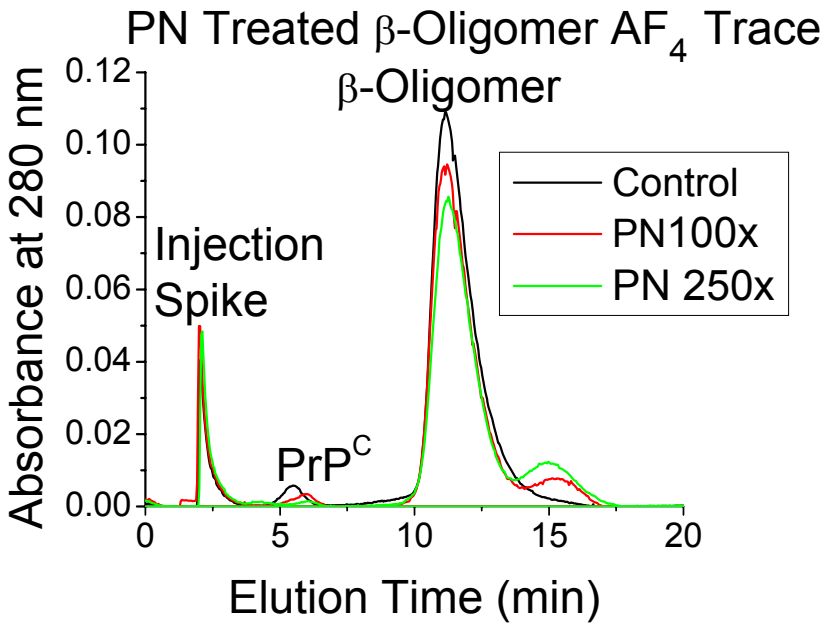

Figure 4-2. AF_4 trace of PN treated β–oligomer.

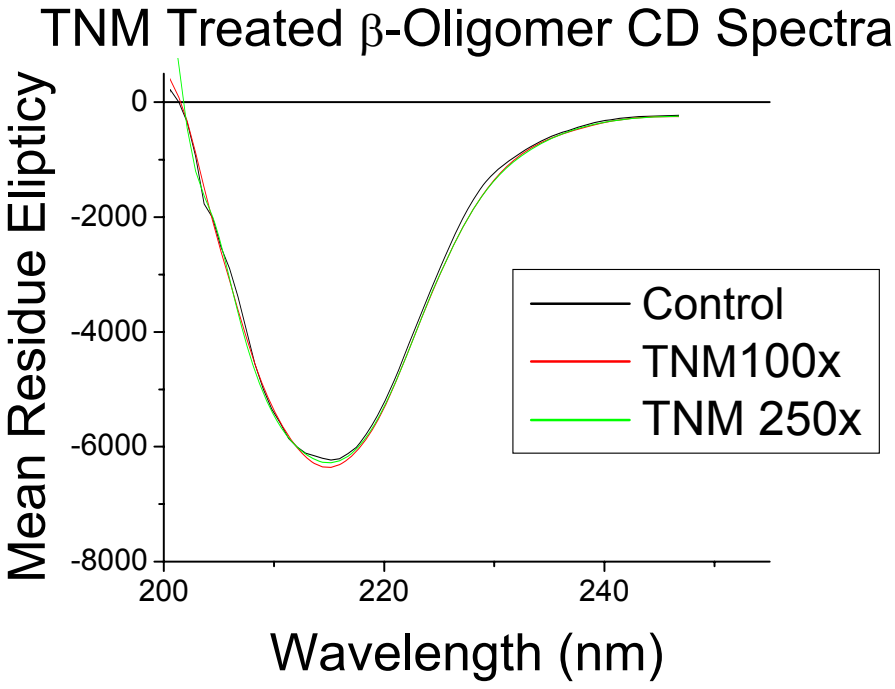

Figure 4-3. CD spectra of TNM treated β–oligomer.

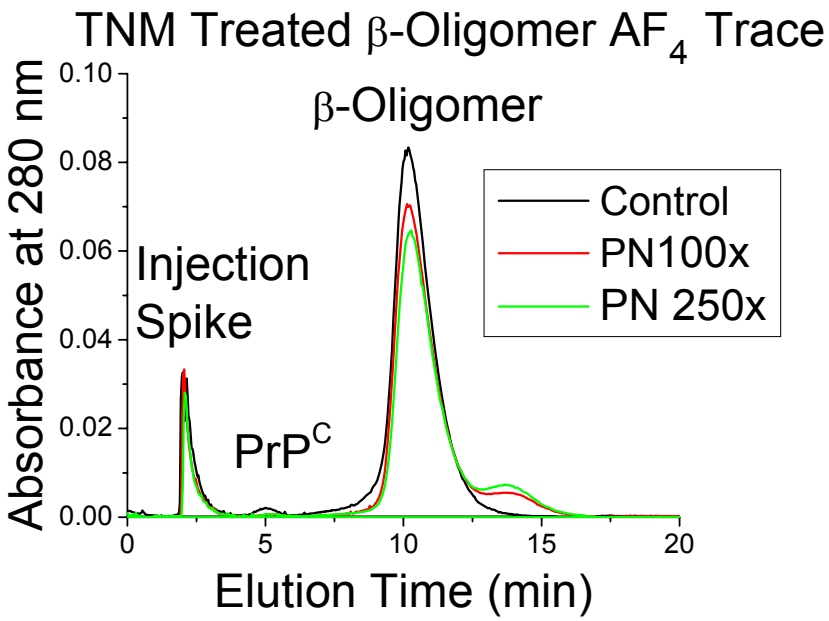

Figure 4-4. AF_4 trace of TNM treated β–oligomer.

Covalent cross-linking: The AF_4 elution traces for 100 and 250-fold PN or TNM treated β–oligomer show the formation of higher mass species. SDS-PAGE on the 250X samples shows that these higher mass species are aggregates of covalently cross-linked PrP (figure 4-5). In the case of the β–oligomer, it was possible to determine whether covalently cross-links were occurring within a single β–oligomer molecule. The AF_4 peak at the elution time corresponding to the single β–oligomer subunit was purified and subjected to SDS-PAGE. This analysis showed that cross-links were forming within a single β–oligomer molecule (figure 4-5),

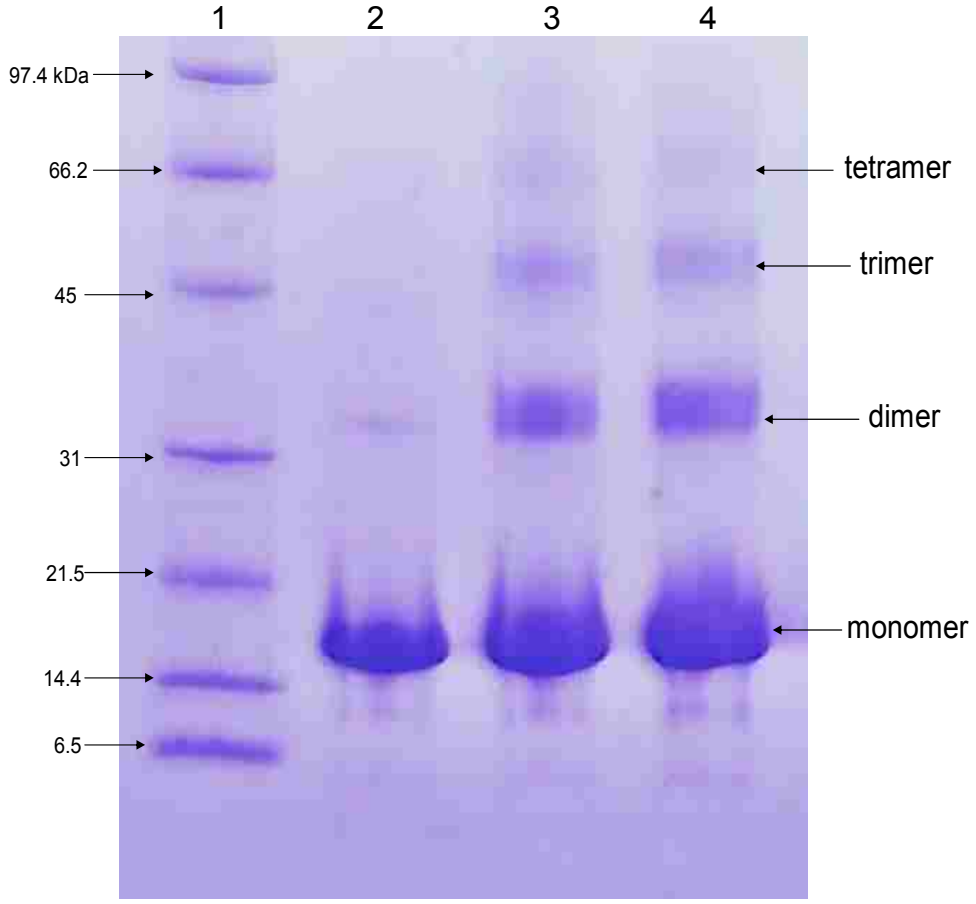

Figure 4-5. SDS/PAGE of the β-oligomer. Lanes: BioRad SDS broad range standard (1), Untreated β-oligomer (2), 100X PN treated β-oligomer (3), 100X TNM treated AF_4 purified β-oligomer (4).

The β–oligomer labeling pattern with PN and TNM: The β–oligomer nitration patterns for 100-fold PN and 100-fold TNM treatment are summarized in table 4-1. The results represent an average of three separate nitration +experiments.

Tryptic Peptide Sequence		**100x PN β-oligomer**	**100x TNM β-oligomer**
P1 (residues 111-136) HMAGAAAAGAVVGGLGG**Y**$_{128}$M LGSAMSR		**+**	**-**
P2 (residues 149-151) **Y**$_{149}$**Y**$_{150}$R	Mono-nitration	**+++**	**+++**
	Di-nitration	**-**	**-**
P3 (residues 157-164) **Y**$_{157}$PNQV**Y**$_{162}$ **Y**$_{163}$R	Mono-nitration	**+**	**++**
	Di-nitration	**-**	**-**
	Tri-nitration	**-**	**-**
P4 (residues 165-185) PVDQ**Y**$_{169}$NNQNNFVHDCVNITIK		**+**	**+**
P5 (residues 209-220) VVEQMCTTQ**Y**$_{218}$QK		**++**	**++**
P6 (residues 221-229) ESQA**Y**$_{225}$**Y**$_{226}$ DGR	Mono-nitration	**++**	**++**
	Di-nitration	**-**	**-**

Table 4-1. MALDI/TOF analysis of Tyr-containing PrP peptides produced by trypsin digestion. Nitration Key: **-**, 0 to 5% nitration; **+**, 6 to 20% nitration; **++**, 21 to 45% nitration; **+++**, 46-70%, **++++**, 71 to 100% nitration.

With 100-fold PN treatment, labeling occurred at Y128, mono-

nitration on the 149-151 peptide containing two tyrosines, mono-nitration on the 157-164 peptide containing three tyrosines, Y169, Y218, and mono-nitration on the 221-229 peptide containing two tyrosines. At 100-fold TNM treatment, the β–oligomer follows the same labeling pattern with the exception of Y128, which was not labeled by TNM.

With both treatments, the highest levels of nitration occurred on 149-151 peptide, followed next by the 221-229 peptide. A MALDI-TOF spectrum of peptides from the tryptic digest of the β–oligomer, after reaction with 100X PN (figure 4-6) as well as a portion of this spectrum enlarged showing the nitration levels of the 157-164 and 221-229 peptides (figure 4-7) is provided. Figures 4-8 and 4-9 show the MALDI_TOF spectra after reaction with 100X TNM.

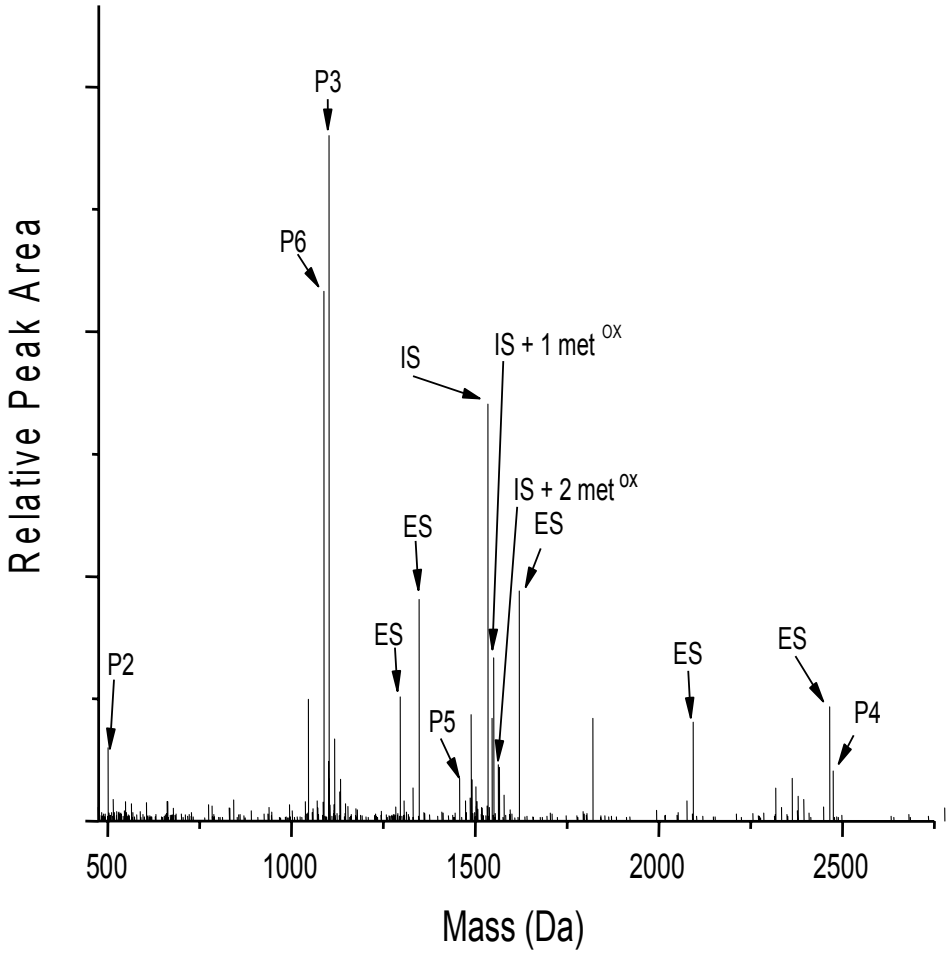

Figure 4-6. A partial MALDI-TOF spectrum of peptides from the tryptic digest of the β–oligomer, after reaction with 100x PN. P2-P6 = tyrosine containing tryptic peptides (P1 observed in different MALDI-TOF mode), IS = internal standard, ES = Bruker external protein standards (listed in table 2-2).

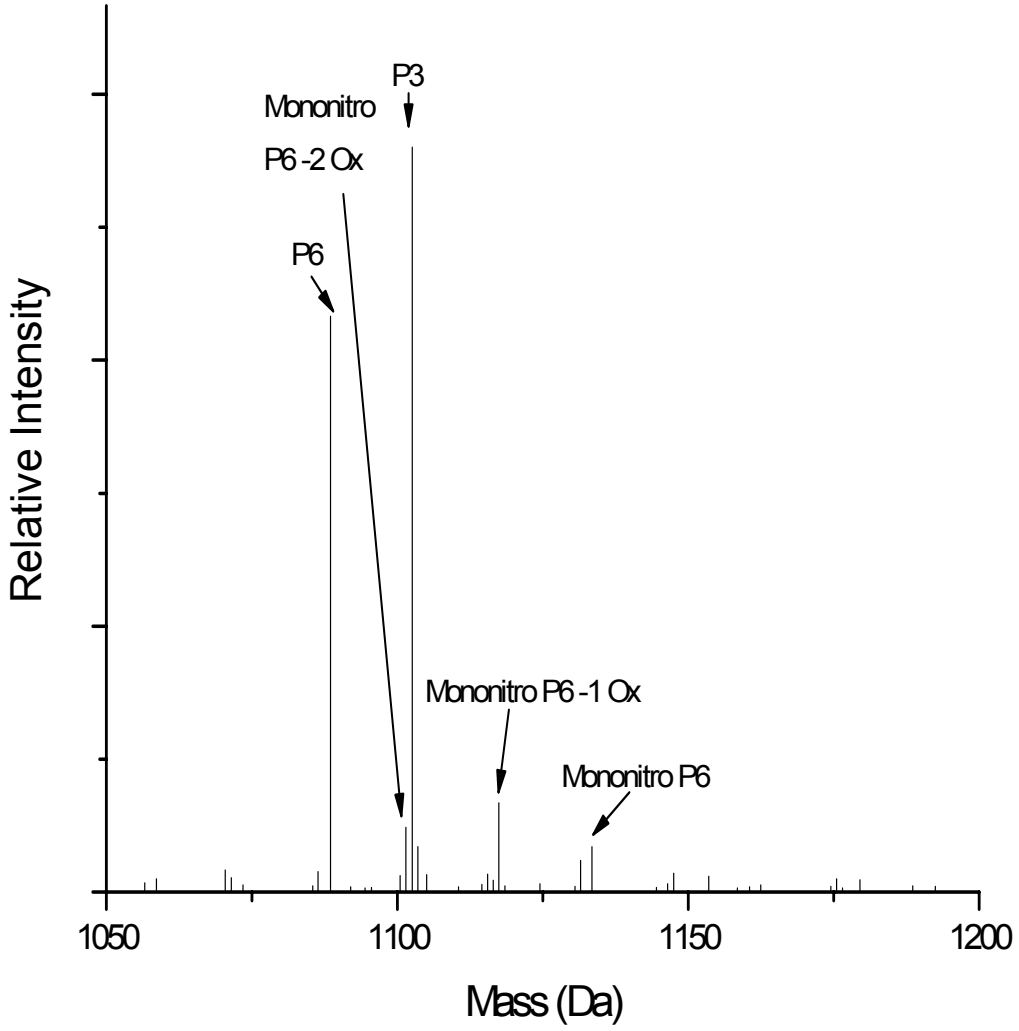

Figure 4-7. The partial MALDI-TOF spectrum showing the loss of one or both oxygens from the nitro-group for P6 as well as the overall levels of nitration for P3 and P6. P2-P6 = tyrosine containing tryptic peptides (P1 observed in different MALDI-TOF mode), IS = internal standard, ES = Bruker external protein standards (listed in table 2-2).

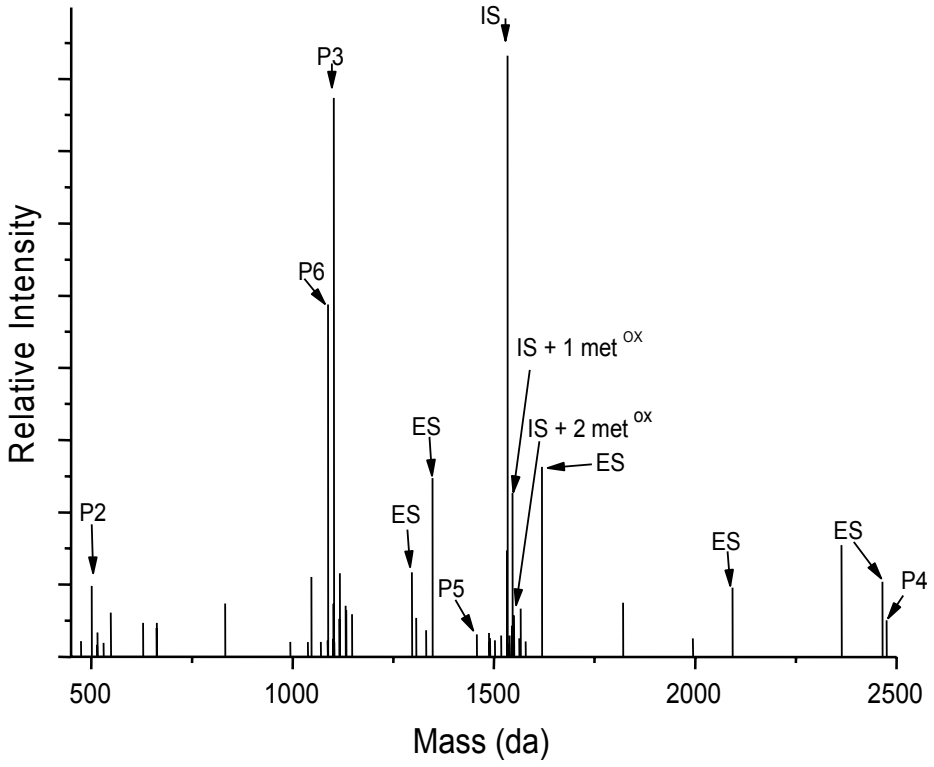

Figure 4-8. A partial MALDI-TOF spectrum of peptides from the tryptic digest of β–oligomer, after reaction with 100X TNM. P2-P6 = tyrosine containing tryptic peptides (P1 observed in different MALDI-TOF mode), IS = internal standard, ES = Bruker external protein standards (listed in table 2-2).

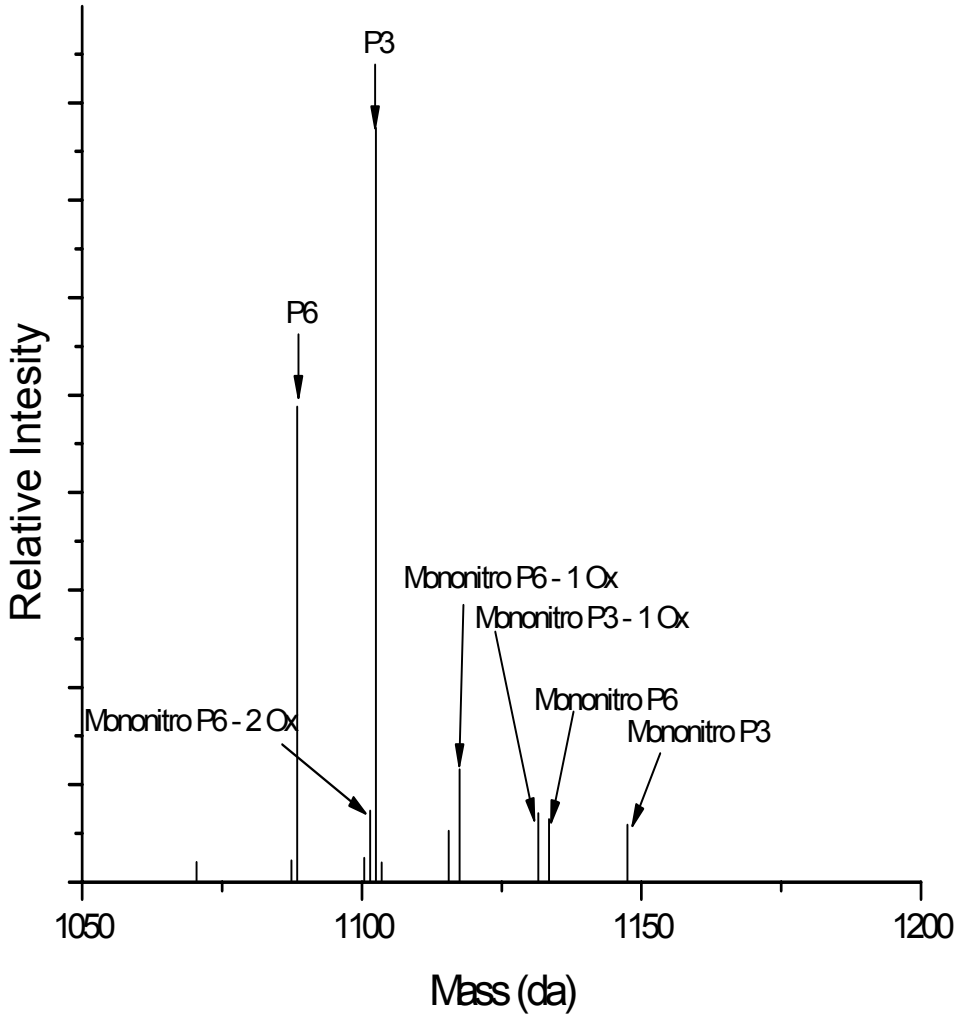

Figure 4-9. Portion of the partial MALDI-TOF spectrum in figure 4-8 to show the loss of one or both oxygens from the nitro-group as well as the levels of nitration for P3 and P6. P2-P6 = tyrosine containing tryptic peptides (P1 observed in different MALDI-TOF mode), IS = internal standard, ES = Bruker external protein standards (listed in table 2-2).

Electro Spray Ionization Tandem Mass Spectrometry: Protein sequencing tandem MS-MS (ESI-MS/MS) was performed by Dr. Holly Cox for the β-oligomer for peptides containing more than one tyrosine residue. Sequencing results indicate that the 157-164 peptide labels at Y162 and

Y163, with no nitration observed at Y157 (figure 4-10). Nitration is seen at both Y225 and Y226 of the 221-229 peptide. In the case of Y149 and Y150, both were reactive as well.

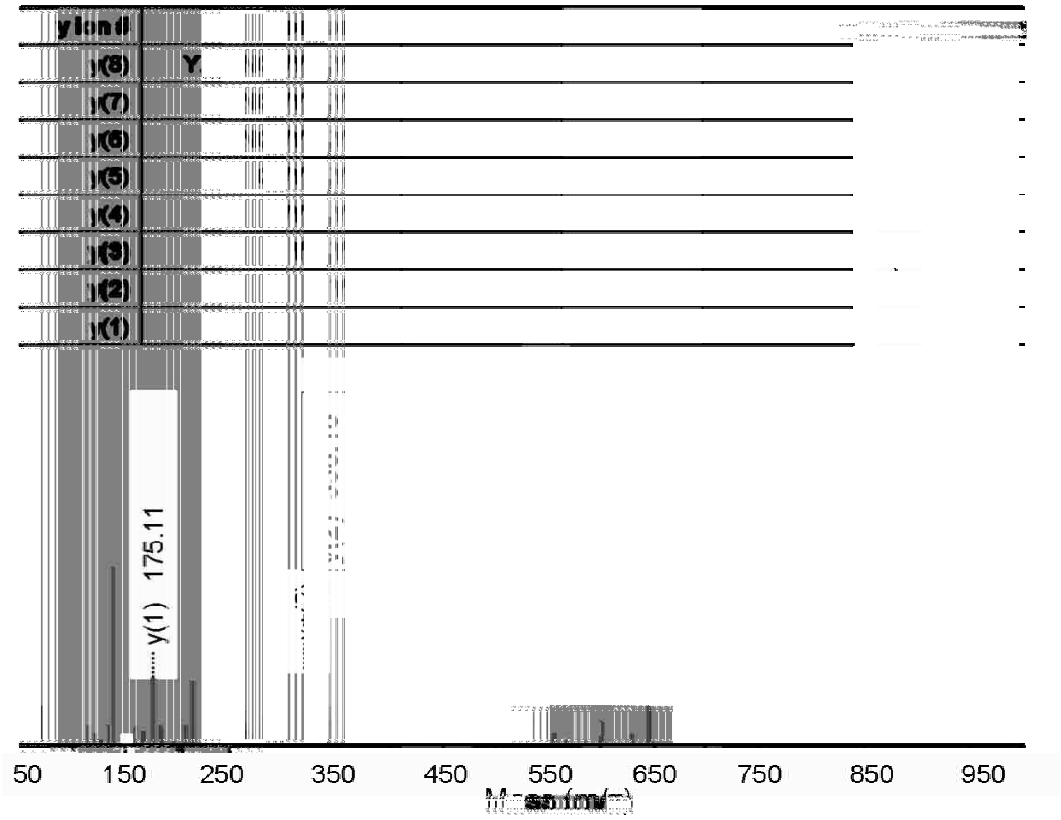

Figure 4-10. A sample ESI-MS/MS spectrum of one mono-nitrated P3 peptide (identified as nitroY162) from the 100-fold PN treated β-oligomer sample. Inset: the masses of the M+H y ions expected from each of the three potential sites of mono-nitration. (*) the loss of ammonia (-17) from R or Q; (++) doubly charged ions.

CD Deconvolution: The deconvolution of the β-oligomer was performed and the results are summarized in table 4-2. Because no crystal or NMR structures are known for the β-oligomer, the precision of

this deconvolution is unknown. However, it is clear that the amount of α-helix secondary structure was low and β-sheet secondary structure was high.

	PrP^C		**β-oligomer**
Secondary Structure Type	From NMR	From CD	From CD
Helix	45%	36%	8%
β-sheet	6%	20%	33%
Turn	15%	19%	25%
Coil	34%	25%	34%

Table 4-2. Deconvolution analysis of the CD spectra of PrP^C and the β-oligomer using the online server DICHROWEB.

Discussion

Considering that low pH is predicted to inhibit the reactivity of TNM, it is surprising that the β-oligomer reacts as efficiently with TNM as with

PN at 100-fold excess. This is especially surprising because such high levels of TNM were required to label PrP^C. Furthermore, TNM causes cross-linking in the β-oligomer (unlike PrP^C) to a similar degree as with PN. The β-oligomer is also able to withstand treatments of 250-fold PN and TNM without any significant loss in secondary structure. These results suggest that the β-oligomer is able to withstand higher levels of nitration without unfolding when compared to PrP^C.

As expected, the nitration pattern of the β-oligomer is different than PrP^C. Two areas in particular show a significant change upon oligomerization. First, high levels of nitration are observed on the 149-151 peptide (containing the first YYR motif) which showed no reactivity in PrP^C. Next, much lower levels of nitration seen were seen at the three carboxy-terminal tyrosine residues (Y225 and Y226). The implications of these differences to PrP^{Sc} structure, as well as an in-depth comparison of all the isoforms, is the subject of Chapter 6.

CD deconvolution shows that there is a large reduction in α-helix and a large increase β-sheet secondary structure when PrP^C converts to form the β-oligomer (table 4-2). The predictions of secondary structure derived from the deconvolution of the CD spectrum do not exactly match NMR solution structure, although the α-helical content agrees well. Clearly, a large decrease in α-helix occurs along with an increase β-sheet secondary structure.

Remarkably, the FT-IR spectra of the β-oligomer and PrP^F are

nearly identical [43]. However, the amount of α-helix estimated by FT-IR is much higher than that determined by deconvolution of the CD spectrum of the β-oligomer. A possible explanation for this difference is that CD spectroscopy more accurately estimates α-helix content while FT-IR spectroscopy more accurately estimates β-sheet character [45].

The conclusion made in Chapter 3 that highly solvent exposed tyrosine residues will likely become nitrated is important for interpreting data for the β-oligomer and PrP^F. In Chapter 6 where all the isoforms are compared, the implications will be further discussed.

CHAPTER 5: PrP^F

Introduction

PrP^{Sc} is a isoform enriched in β-sheet secondary structure that forms insoluble fibrils associated with infectivity [1]. As described earlier, no NMR or crystal structures exist for PrP^{Sc}. PrP^F is the recombinant form of PrP^{Sc} fibers associated with much lower levels of infectivity [6].

Structural details of the PrP^{Sc} isoform as a whole have not yet been determined, although regions have been determined to ~7 Å [46]. As described in Chapter 1, PrP^{Sc} forms large heterogeneous aggregates, and so traditional methods such as NMR and X-ray crystallography have been unsuccessful. A detailed structure of the PrP^{Sc} fiber subunits is of utmost importance to the treatment and prevention of not only prion diseases, but all amyloid plaque disorders in general. In this current study, we seek to describe molecular level details of PrP^F through nitration with peroxynitrite (PN) coupled to mass spectrometry.

In the absence of a precise structure for PrP^{Sc}, many studies have focused on elucidating gross PrP^{Sc} structural characteristics [47-60]. Atomic force microscopy and X-ray diffraction studies have revealed that a common morphology exists for all amyloid fibrils [47, 48]. So called "protofilaments", with diameters ranging from 1.2-3.8 nm, intertwine with one another to form the larger fibril structure. Regardless of the precursor protein studied, these protofilaments appear to be the building blocks of all

amyloid fibrils.

Using proteinase K, a non-specific serine protease that cleaves on the carboxylic sides of aliphatic, aromatic or hydrophobic residues, it has been shown that PrP^{C} and PrP^{Sc} fibrils display differential digestion profiles [48,49]. Specifically, while PrP^{C} remains sensitive to complete proteolysis, PrP^{Sc} fibrils are only subject to amino-terminal proteolysis and form a resistant core from amino acids ~90-232. This finding as well as amino-terminal deletion studies have led to the determination that amino-terminal region of the prion protein is not necessary to form PrP^{Sc} [53-55], although it does influence the process [53-56].

Antibody studies have identified selective epitopes that are exposed only in PrP^{Sc} [25, 57, 58]. In one antibody study carried out by Cashman and colleagues [25], the investigators identified a YYR motif as a PrP^{Sc} specific epitope. In the primary structure of PrP 90-232, two YYR motifs are present at amino acids 149-151 and 162-164. Although the study did not determine which motif became exposed upon conversion to PrP^{Sc}, or if both YYR motifs were antigenic, the authors did favor assignment to the second YYR (residues 162-164). In this same study, using fluorescence spectroscopy, the authors suggest that upon conversion from PrP^{C} to PrP^{Sc}, more tyrosine residues become surface exposed.

In another more recent study [58] using a number of different antibody fragments and antibodies, it was shown that the region

encompassing amino acids 132-156 was more immunogenic than regions 159-174 or 224-230 in PrP^{Sc}. These results suggest, contrary to Cashmann and colleagues assessment, that the first and not the second YYR motif is antigenic in PrP^{Sc}.

Fourier transform infrared spectroscopy (FT-IR) has indicated that a large increase in β-sheet and a slight decrease in α-helix and random coil secondary structure occurs in the transition from PrP^{C} to PrP^{Sc} [59, 60]. As stated in Chapter 4, CD spectroscopy more accurately estimates α-helix content while FT-IR spectroscopy more accurately estimates β-sheet character [45]. Therefore, the amount of α-helix secondary structure present in PrP^{Sc} may be much lower than FT-IR measurements suggest and may be much closer to the β-oligomer.

Solid state NMR studies of the murine PrP89-113 peptide confirmed that this region is entirely β-sheet when in the fibrillar form [46]. Low resolution 2-D electron crystallography has also been used to probe PrP^{Sc} and found that the fibrils are consistent with parallel β-helices [60].

From data gathered in these studies and others, a number of models have been proposed as the structure of the PrP^{Sc} subunits [61-68]. Although each of these models differs in the particular residues studied and data used, every model proposes that interacting β-strands between misfolded subunits serves as the mechanism of aggregation. Two of the leading subunit models in the field are the β-spiral model [62] and the β-helix model [63]. Both models omit much of the protease sensitive amino-

terminus and focus on the resistant core (residues 109-219 for the β-spiral model and 90-228 for the β-helix model). Each predicts that the increased β-sheet character occurs in amino-terminus of PrP^C, leaving much of the carboxy-terminal α-helical character unchanged. Figure 5-1 displays the two different models.

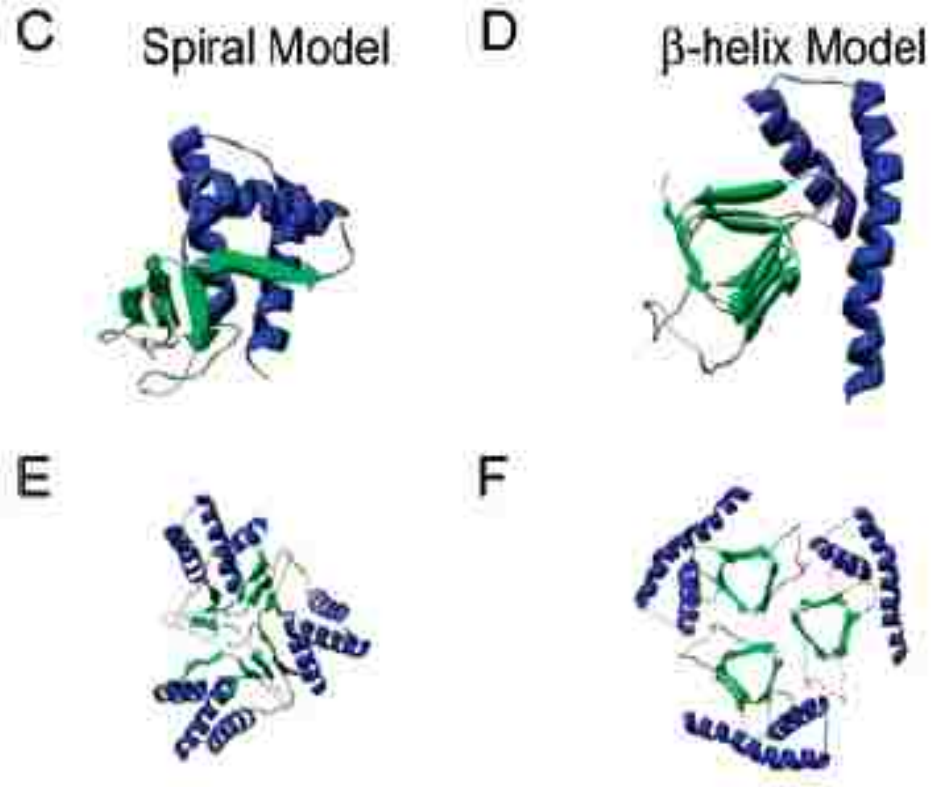

Figure 5-1. The β-spiral model [61] and the β-helix model [62] for the PrP^{Sc} fibril subunit. Figure is taken directly from reference 67(used with permission).

The β-spiral model was generated by using molecular dynamics simulations conducted under the cellular conditions, namely low pH, in which the misfolding and aggregation of PrP^C is thought to take place. The β-spiral subunit consists of three α-helices and four β-strands. Three of

the four β-strands form a small β-sheet, whereas the fourth β-strand is located on a different face of the monomer. Interactions between the three β-strands of one monomer and the lone β-strand from another monomer form the subunit interface. Each subunit stacks on top of the next, growing in a chain, to form a spiral reminiscent of a winding staircase.

The β-helix model was constructed after threading the prion sequence onto several known β-sheet folds and choosing the fold that best fit the available data. A fold known as the left-handed β-helix was selected. The β-helix model predicts that the amino-terminus up to the second α-helix (residues 90-175 in model) is essentially converted to a left-handed β-helix (see figure 5-1). Three monomers come together such that the left-handed β-helices form a core. Other trimers are proposed to stack directly upon another to propagate the chain. It should be noted that the energetics of this model have been called into question [68] because of the lack of plausible interactions to hold the trimer subunits together, and to stack them on top of one another.

The β-spiral model and β-helix model were compared recently by Daggett and colleagues [68]. Although this comparison was objective, it should be noted that the β-spiral model was constructed by DeMarco and Daggett. In the assessment, the authors examined all of the experimental data available and came to the conclusion that while the β-spiral model was consistent with all, the β-helix model could not account for some of the experimental data.

For the same reason that it can't be stated that the β-oligomer has a similar overall structure as PrP^{Sc}, we must accept that is also true when comparing PrP^{Sc} and PrP^{F}. Again, no high resolution (within a 1.5-3 Å) molecular structures have been solved for PrP^{F}. However, because PrP^{Sc} and PrP^{F} share more physical characteristics than PrP^{Sc} and the β-oligomer and PrP^{F} has been associated with infectivity [7], it is likely that PrP^{F} represents a better model of PrP^{Sc}.

Materials and Methods

A detailed description of the materials and methods used is provided in Chapter 2. Briefly, PrP^{F} was treated with varying levels of PN. Samples treated with 100-fold PN were analyzed by electron microscopy to ensure no structural changes had occurred and MALDI-TOF mass spectrometry to determine which tryptic peptides became nitrated. Samples treated with up to 1000-fold PN were analyzed by SDS/PAGE to determine if any covalent cross-links between PrP monomers were present.

Results

PrP^{F} sensitivity to treatment with 100-fold PN : Following treatment with 100-fold PN, electron micrographs were taken of PrP^{F}. After treatment, no change was detected in the structure of the fibrils according to EM (figure 5-2).

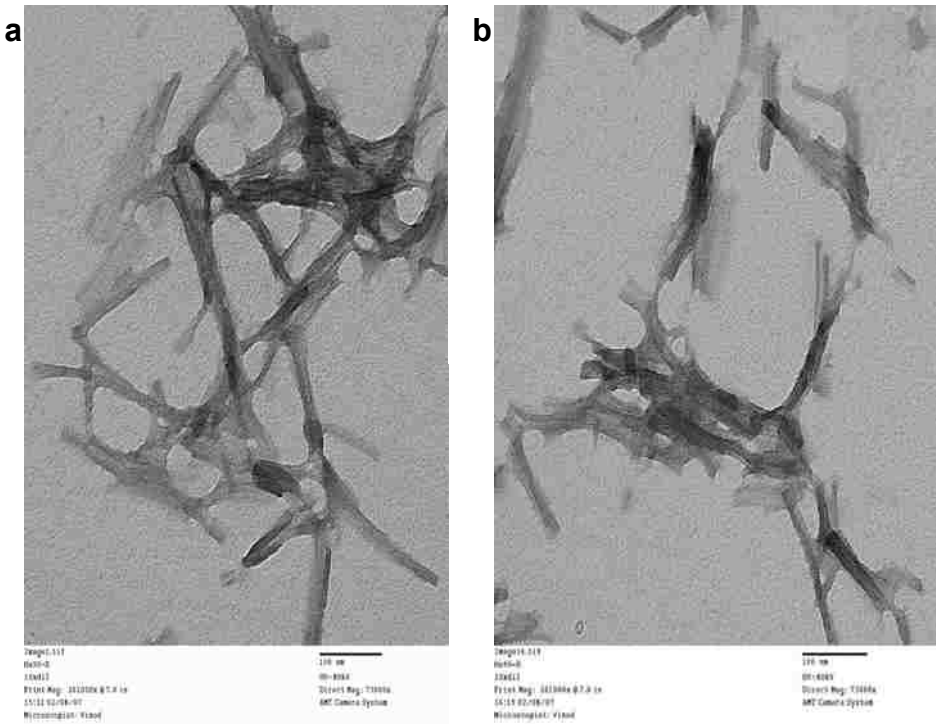

Figure 5-2. Electron micrographs of (a) untreated and (b) 100-fold peroxynitrite treated (b) PrP^F. Images were taken at the Rocky Mountain Laboratories Electron Microscopy facility under the direction of Dr. Roger Moore (Bar = 100 nm).

Covalent cross-linking: Covalent Cross-linked PrP monomers were detected by SDS/PAGE following PrP^F treatment with1000-fold PN at pH 7.5. 1000-fold PN was used to maximize the cross-linking reaction. No mass spectrometry was performed on this sample.

1 2 3

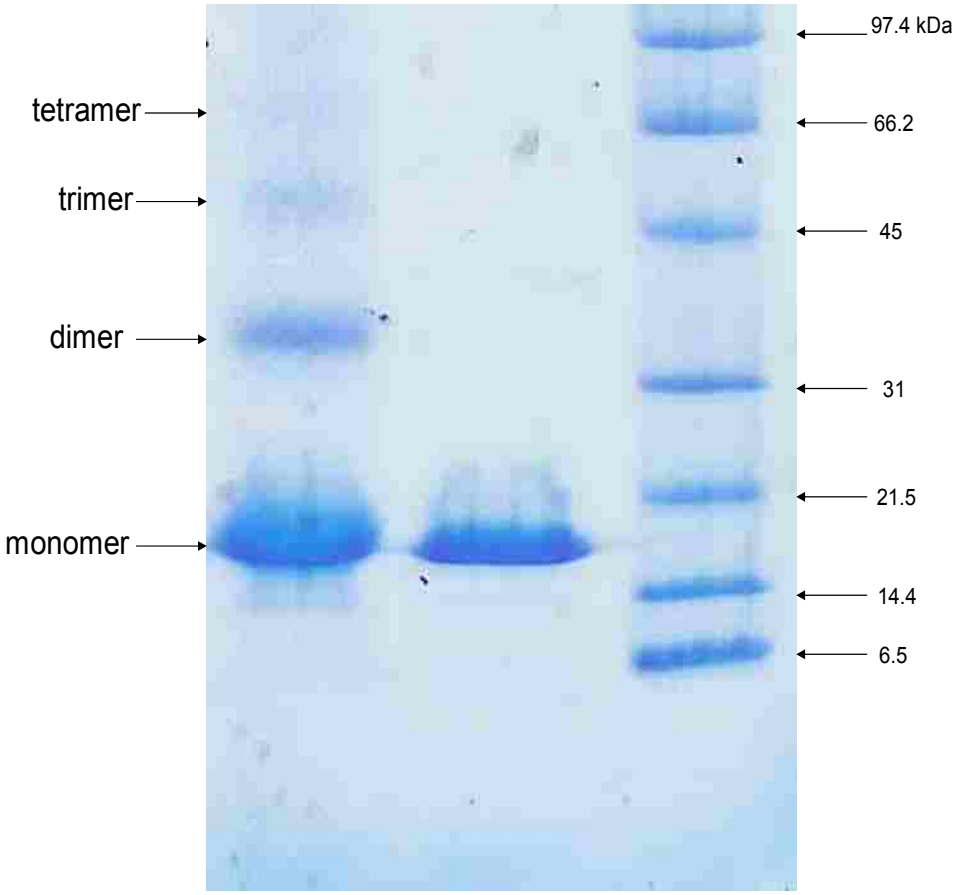

Figure 5-3. SDS/PAGE of PrP^F. Lanes: 1000X PN treated PrP^F (1), Untreated PrP^F (2), BioRad SDS broad range standard (3)

The PrP^F labeling pattern with PN: The PrP^F nitration patterns for 100-fold PN treatment is summarized in table 5-1. The levels indicated represent an average for three separate experiments

Tryptic Peptide Sequence	**100x PN pH 5.5**	**100x PN pH 7.5**

		PrP^F	PrP^F
P1 (residues 111-136) HMAGAAAAGAVVGGLGG**Y_{128}**M LGSAMSR		**++**	**++**
P2 (residues 149-151) **$Y_{149}Y_{150}$**R	Mono-nitration	**++**	**+++**
	Di-nitration	**-**	**-**
P3 (residues 157-164) **Y_{157}**PNQV**Y_{162}** **Y_{163}**R	Mono-nitration	**+**	**+**
	Di-nitration	**-**	**-**
	Tri-nitration	**-**	**-**
P4 (residues 165-185) PVDQ**Y_{169}**NNQNNFVHDCVNITIK		**-**	**-**
P5 (residues 209-220) VVEQMCTTQ**Y_{218}**QK		**+++**	**+++**
P6 (residues 221-229) ESQA**$Y_{225}Y_{226}$** DGR	Mono-nitration	**++**	**++**
	Di-nitration	**-**	**-**

Table 5-1. MALDI/TOF analysis of Tyr-containing PrP peptides produced by trypsin digestion. Nitration Key: **-**, 0 to 5% nitration; **+**, 6 to 20% nitration; **++**, 21 to 45% nitration; **+++**, 46-70%, **++++**, 71 to 100% nitration.

With 100-fold PN treatment at both pH 5.5 and pH 7.5, labeling occurred at Y128, mononitration on the 149-151 peptide containing two tyrosines, mononitration on the 157-164 peptide containing three tyrosines, Y218, and mononitration on the 221-229 peptide containing two tyrosines. The nitration pattern was the same at pH 5.5 and pH 7.5. Sequencing of peptides containing multiple tyrosine residues has not been performed for PrP^F.

The highest levels of nitration occurred on the 149-151 peptide, followed next by 111-136 and the 221-229 peptide. A partial MALDI-TOF spectrum of peptides from the tryptic digest of the PrP^F, after reaction with 100x PN, is provided for reference (figure 5-4). A portion of this spectrum showing the nitration levels of the 157-164 and 221-229 peptides is also provided (figure 5-5).

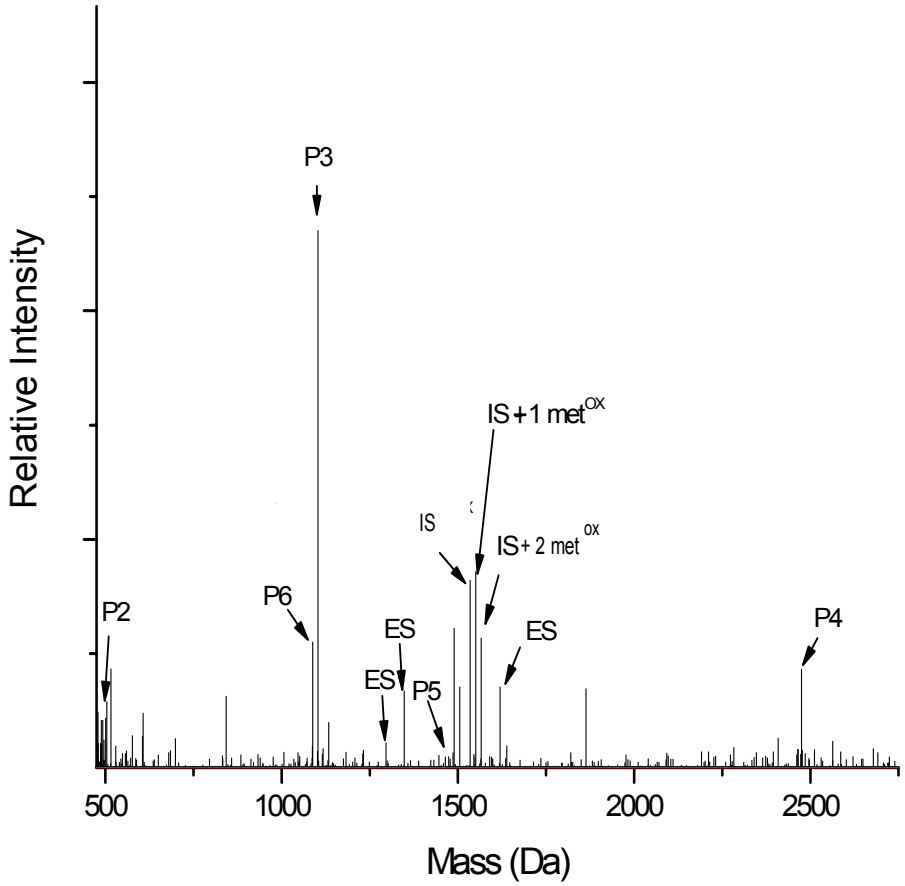

Figure 5-4. A partial MALDI-TOF spectrum of peptides from the tryptic digest of PrP^F, after reaction with 100x PN. P2-P6 = tyrosine containing tryptic peptides (P1 observed in different MALDI-TOF mode), IS = internal standard, ES = Bruker external protein standards (listed in table 2-2).

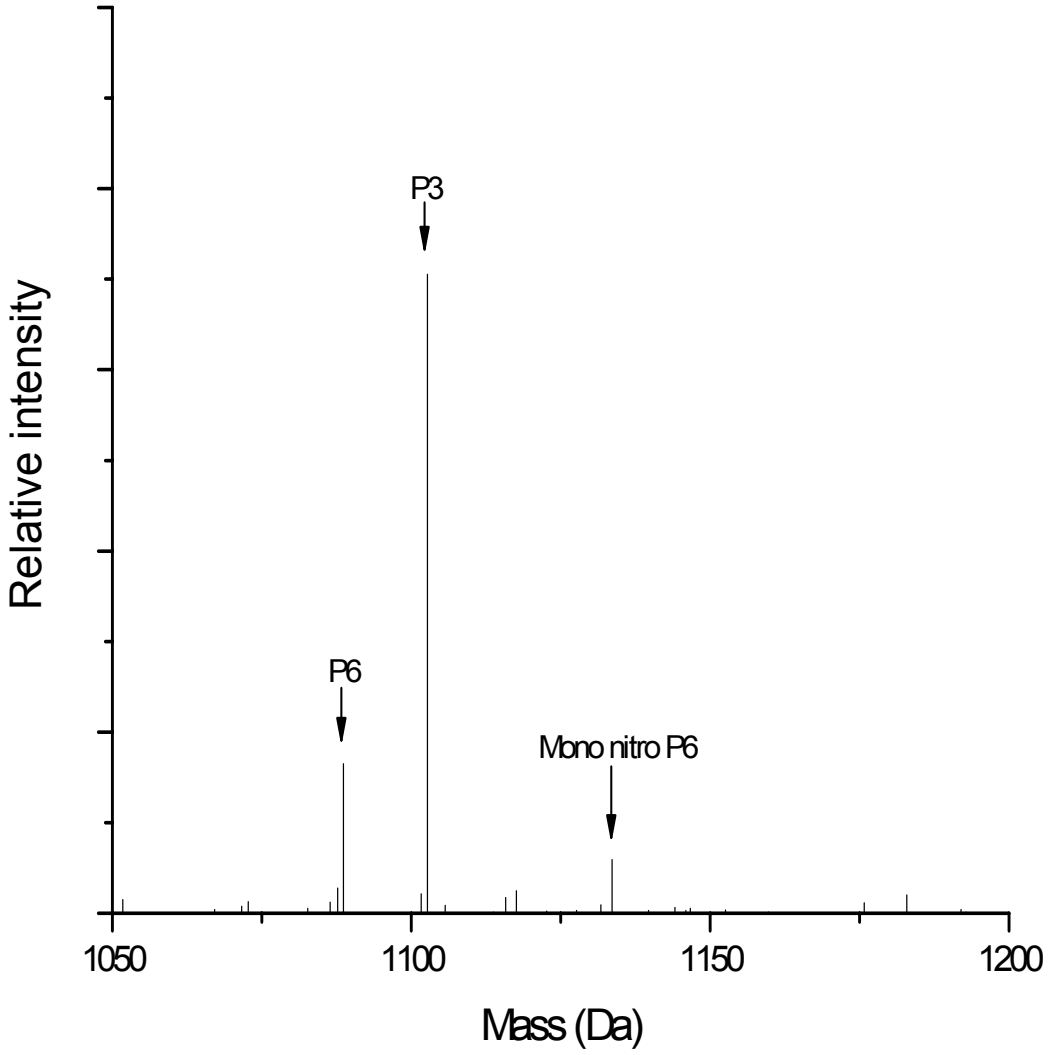

Figure 5-5. Portion of the partial MALDI-TOF spectrum in figure 5-4 to show the loss of one or both oxygens from the nitro-group as well as the levels of nitration for P3 and P6. P2-P6 = tyrosine containing tryptic peptides (P1 observed in different MALDI-TOF mode), IS = internal standard, ES = Bruker external protein standards (listed in table 2-2).

Discussion

As expected, the nitration pattern of the PrP^F is very different than PrP^C. Remarkably, PrP^F and the β-oligomer have an almost identical nitration pattern according to MALDI-TOF MS (without having sequencing results to confirm). This provides strong evidence that the β-oligomer is a good structural model of PrP^F, and possibly PrP^{Sc}. The implications of these isoform-dependent nitration patterns to prion biophysics, as well as an in-depth comparison of all the isoforms, are the subject of Chapter 6.

The most important similarity between PrP^F and the β-oligomer is the high levels of nitration seen on the 149-151 peptide (containing the first YYR motif) and the low levels of nitration seen on the 157-164 peptide (containing the second YYR motif). The conclusion that the first, and not the second YYR motif is the PrP^{Sc} specific epitope that was suggested by the nitration pattern of the β-oligomer is now a much stronger claim. This evidence is significant because, if extended to the structure of PrP^{Sc}, it provides molecular level details of the aggregated isoform.

The labeling pattern of PrP^F does not significantly change at the two pH levels tested. This result is convenient because it allows us to compare PrP^F to the other isoforms (nitration done at pH 5.5) while still conducting reactions at the physiological pH 7.5. Most importantly reactions at pH 7.5 allow us to extend our comparisons to include PrP^{Sc}.

The electron micrographs of untreated and 100-fold PN treated PrP^F are not different. This is an important structural check to ensure that

the PN treatment did not cause inter-fibril cross-links, which would appear as clumping, or global unfolding of the fibrils, which would have appear as the loss of fibrils.

CHAPTER 6: COMPARING THE DIFFERENT ISOFORMS AND FUTURE DIRECTIONS

Comparing PrP^C, the β-oligomer and PrP^F

The normal prion protein cellular isoform (PrP^C) and the disease associated β-oligomer and PrP^F isoforms were labeled at tyrosine residues with peroxynitrite (PN) and tetranitromethane (TNM). These experiments were done in an attempt to identify structural differences among the three isoforms. From the results, two regions have been identified that undergo substantial changes in the local chemical environment upon the oligomerization of PrP^C. These changes could be a result of conformational changes between the isoforms, or conversely, these changes could be due to the packing of PrP polypeptides in the aggregated isoforms. Remarkably, these changes occur both when PrP^C aggregates to form either the soluble β-oligomer or fibrillar PrP^F. Table 6-1 reports the nitration patterns of PrP^C, the β-oligomer and PrP^F following treatment with 100-fold PN.

Tryptic Peptide Sequence		**100x PN PrP^C**	**100x PN β-oligomer**	**100x PN PrP^F pH 7.5**
P1 (residues 111-136) HMAGAAAAGAVVGGLGG**Y_{128}**MLGSAMSR		**+**	**+**	**++**
P2 (residues 149-151) **$Y_{149}Y_{150}$**R	Mono-nitration	**-**	**+++**	**+++**
	Di-nitration	**-**	**-**	**-**
P3 (residues 157-164) **Y_{157}**PNQV**$Y_{162}Y_{163}$**R	Mono-nitration	**+**	**+**	**+**
	Di-nitration	**-**	**-**	**-**
	Tri-nitration	**-**	**-**	**-**
P4 (residues 165-185) PVDQ**Y_{169}**NNQNNFVHDCVNITIK		**-**	**+**	**-**
P5 (residues 209-220) VVEQMCTTQ**Y_{218}**QK		**+++**	**++**	**+++**
P6 (residues 221-229) ESQA**$Y_{225}Y_{226}$**DGR	Mono-nitration	**++++**	**++**	**++**
	Di-nitration	**++**	**-**	**-**

Table 6-1. MALDI/TOF analysis of Tyr-containing PrP peptides produced by trypsin digestion. Nitration Key: **-**, 0 to 5% nitration; **+**, 6 to 20% nitration; **++**, 21 to 45% nitration; **+++**, 46-70%, **++++**, 71 to 100% nitration.

Within the PrP primary sequence, two YYR (149-151, 162-164) and one YYD (225-227) motifs are present. A previous study using monoclonal antibodies identified a YYR epitope exposed in PrP^{Sc} that is buried in PrP^C [25]. The most striking difference in nitration patterns between PrP^C and both the β-oligomer and PrP^F is in the first YYR. Our current work clearly shows that Y149 and Y150 only become reactive toward nitration upon PrP^C conversion to the β-oligomer or PrP^F. In the case of PrP^F, it is not yet known which (or both) of the tyrosine residues

becomes nitrated.

This finding is in contrast to the conclusions made by Paramithiotis et al. [25], who contend that it is likely residues 162-164 that represent the PrP^{Sc} exposed epitope. Our results show a similar, very low level of mono-nitration at either Y162 or Y163 between PrP^{C} and the β-oligomer with 100-fold PN, 100-fold TNM (β-oligomer), and 1000-fold TNM (PrP^{C}). This same low level of mono-nitration is also detected on the 157-164 peptide of PN-treated PrP^{F} (TNM was not tested). Nitration patterns clearly suggest that the first YYR motif undergoes a dramatic change in chemical environment upon aggregation while the second YYR does not. The result could be due to conformational differences within a polypeptide, packing between polypeptides of a protofibril, or packing between protofibrils.

The nitration patterns of PrP^{C}, the β-oligomer and PrP^{F} point to another region where significant structural change occurs - the carboxy-terminus. Upon oligomerization, a reduction in reactivity occurs at Y225 and Y226 with both nitrating agents in the β-oligomer and PN with PrP^{F}. Reactivity is highest in PrP^{C} at the 221-230 peptide (including large amounts of dinitration), followed by Y218. In all isoforms, Y218 was efficiently nitrated.

The patterns of nitration after 100-fold PN treatment are similar for the β-oligomer and PrP^{F}. Although it was expected that nitration patterns would resemble one another, the nearly identical patterns suggest that

common structural changes occur when PrP^C converts to either of the β-oligomer or PrP^F isoforms. This result also argues against the notion that the changes observed are simply due to subunit packing, rather than conformational differences, as the packing is expected to be quite different between the β-oligomer and PrP^F.

From these results, we can confidently suggest that the β-oligomer serves a valid model for studying PrP^F and PrP^{Sc}. Further support of this conclusion comes from the fact that FT-IR spectroscopy does not predict α-helix secondary structure as well as CD spectroscopy [45]. Because the FT-IR spectra of the β-oligomer and PrP^F are nearly identical [43], it is quite possible that the α-helical content of PrP^{Sc} is less than previously reported 17-30% [59-60] and much closer to the 8% measured by CD reported in Chapter 4.

The reactivity of PN or TNM toward a given tyrosine is dependent on a number of factors [69]. Potassium peroxynitrite (K^+ ONO_2^-) is stable only at high pH. Upon exposure to an acidic environment, the protonation of ONO_2^- induces the formation of $NO_2^{\cdot}$ and $HO^{\cdot}$. The presence of these radicals in the mixture can lead to hydrogen abstraction from a tyrosine residue. Following the radicalization of tyrosine, reaction can occur between $Tyr^{\cdot}$ and $NO_2^{\cdot}$ at the meta positions of the tyrosyl group (or a cross-link between two Tyr radicals). Factors positively influencing the reaction at a particular Tyr are solvent exposure, presence in a loop and proximity to a negative charge or hydrophobic environment. Cysteines

near the tyrosine will reduce the likelihood of nitration. A number of other amino acids react with PN, including: oxidation of cysteine and methionine residues, nitration of tryptophan, hydroxylation of phenlyalanine and possible modification of histidine. Of these, only Met oxidation was observed. When appropriate to determining sites of nitration, the possible oxidation of methionine was accounted for.

TNM ($C(NO_2)_4$) nitrates tyrosine residues using a different mechanism than that described for PN [70-71]. In the case of TNM, the entire molecule encounters a tyrosine and a charge transfer complex forms. Electrophilic attack leads to the formation of nitrotyrosine. As with PN, protein cross-links can occur via the meeting of two tyrosine radicals. Because this mechanism requires the initial abstraction of a proton from the hydroxyl group of a tyrosine, the nitration rate increases as the pKa of the Tyr residue decreases. This mechanism also suggests that the reactivity of a Tyr should increase if it is involved in a hydrogen bond or is proximal to a positive charge. Predicting the reactivity of a Tyr with TNM is not cut and dry; the microenvironment of each residue must be considered. One study found that the rate of reaction with TNM appears to increase with surface exposure and decrease when the microenvironment is negatively charged or hydrophobic [72]. However, authors of an earlier study contend that the microenvironment drives TNM reactivity independent of solvent exposure [70].

The complete absence of reactivity in PrP^C at Y149 and Y150

strongly suggests that an overall structural change must occur to make both the β-oligomer and PrP^F reactive at one or both of these residues. When taken together with previous antibody work, Y149 and Y150 likely represent a region of PrP^C that undergoes significant structural change during misfolding and oligomerization. The reduction in reactivity of the carboxy-terminal tyrosines at positions 225 and 226 is also indicative of a region in which a large structural change likely occurs upon oligomerization or packing. Recent evidence using recombinant fibrils suggests that the 224-230 epitope is buried under native conditions [58].

Residues 149-151 are located on helix 1 of the PrP^C, a region that is predicted to undergo complete transformation in the β-helix model [63]. Y149 and Y150 are predicted to be highly surface exposed in the β-helix model as well. On the other hand, Y225 and Y226 are also highly surface exposed in the β-helix model, which is not consistent with our results (figure 6-1). Table 6-2 shows the predicted solvent accessible surface area (SASA) for PrP^C and the β-helix model.

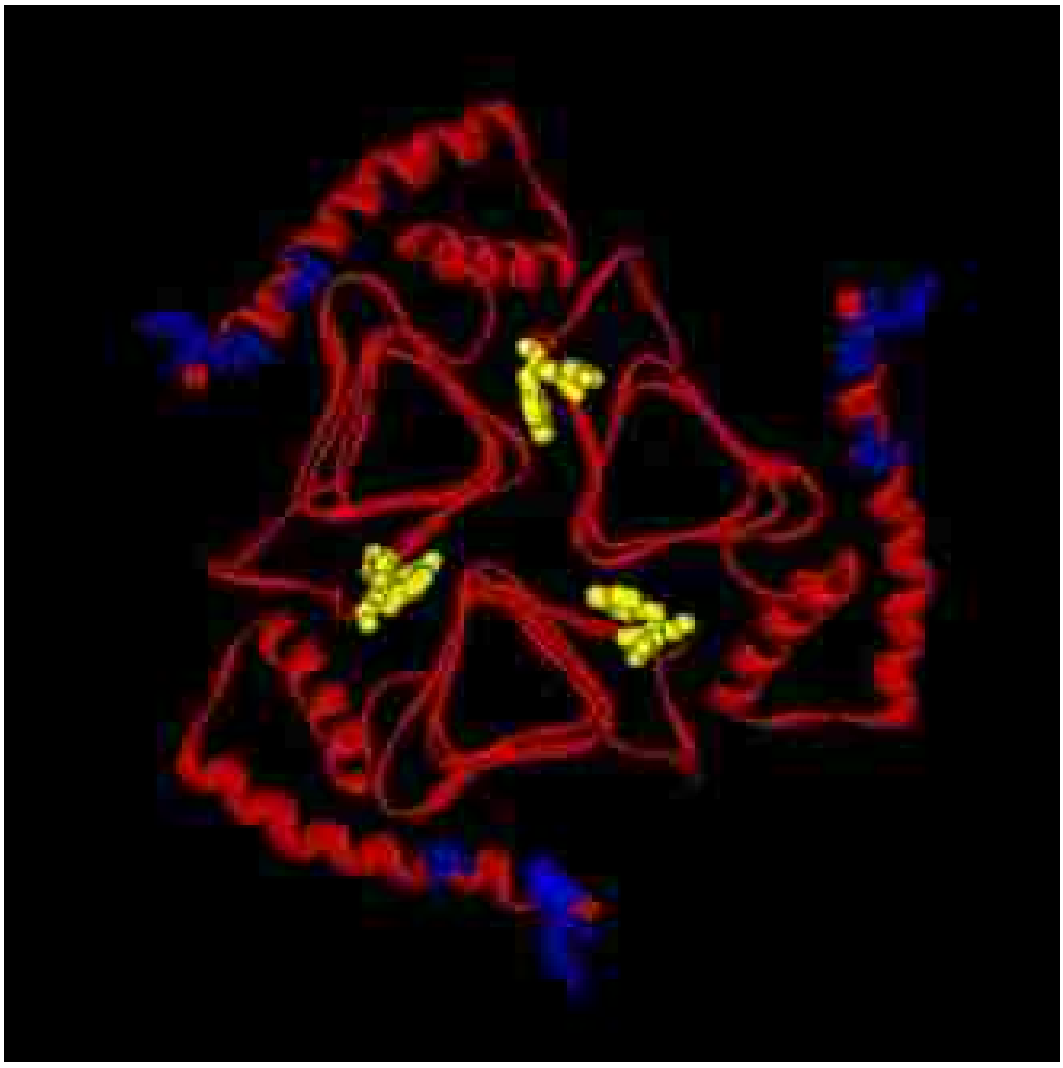

Figure 6-1. The β-helix model [61] with tyrosines 149 and 150 yellow colored in and tyrosines 218, 225 and 226 colored in blue.

Tyrosine residue	128	149	150	157	162	163	169	218	225	226
PrP^C SASA%	5.6	13.7	2.8	2	11.7	3.3	16.4	5.6	39	59
β-Helix SASA%	1.1	42	40.2	44.3	12.3	43.9	31.5	38.5	59.6	58.6

Table 6-2. Solvent accessible surface area (SASA) for PrP^C, β-spiral model, and the β-helix model. SASA calculations were generated by the MOLMOL program using PDB coordinates from PrP^C [20] and the β-helix model [63].

To summarize our most important findings, we have identified two regions of PrP^C that undergo considerable conformational change in the aggregation process. In both the aggregated isoforms studied, the β-oligomer and PrP^F, the chemical environments of the first YYR motif and the carboxy-terminus are dramatically different from PrP^C.

Future Studies

A number of future studies branching directly from these nitration experiments will provide important structural details about PrP^{Sc}. This information could be very useful in the construction of models of the infectious PrP^{Sc} fibrils and thus give crucial information about the formation of infectious prions.

First and foremost, sequencing mass spectrometry should be performed on the 100-fold PN treated PrP^F. Although this is more completion of existing work than a future study, it is the needed step prior to publishing the PrP^F data and is currently being conducted in the McGuirl laboratory. This data will show specifically which of the tyrosine residues that are becoming nitrated in PrP^F, as well as provide a better

understanding of how closely related the β-oligomer is to PrP^{F}.

Next, the nitration pattern of PrP^{Sc} should be characterized using the same techniques described for PrP^{C}, the β-oligomer and PrP^{F}. This will be more technically difficult, as PrP^{Sc} isolated from brain homogenate is glycosylated, which could interfere with the nitration reagents. If quality data could be gathered, then the information would provide molecular level details of PrP^{Sc} and would be invaluable in assessing models of the structure of PrP^{Sc}.

Another important set of experiments is to determine the cross-linking sites of the β-oligomer, PrP^{F}, and possibly PrP^{Sc}. By exploiting this side reaction as a stand-alone technique, the physical constraints of these aggregated isoforms can be partially defined. The main problem associated with this approach is that cross-linking is a side reaction and obtaining enough sample to perform mass spectrometry may be difficult. Even with enough sample, there are a large number of potential cross-link sites (i.e., many masses to look for) that will complicate matters even further.

Finally, antibodies should be used probe PrP^{C}, the β-oligomer, PrP^{F} and PrP^{Sc} before and after nitration. By the disruption of binding at selective epitopes, solvent accessibility can be more or less directly correlated to nitration by PN and TNM. Although this approach appears relatively straight-forward, the precise epitope to which an antibody binds may not be clear, leaving the possibility for incorrect results.

APPENDIX

Masses of Tyr-Containing PrP peptides and Respective Nitration and Oxidized Methionine Derivatives

P1: 111-HMAGAAAAGAVVGGLGG**Y**MLGSAMSR-136					
	peptide	+1 Oxidized Met	+ 2 Oxidized Met	+ 3 Oxidized Met	
No nitration	2364	2380	2396	2412	
Nitro	2409	2425	2441	2457	
Nitro -1 Ox	2393	2409	2425	2441	
Nitro -2 Ox	2377	2393	2409	2425	
P2: 149-**YY**R-151			P3: 157-**Y**PNQV**YY**R-164		
	peptide			Peptide	
No nitration	501		No nitration	1103	
Nitro	546		Nitro	1148	
Nitro -1 Ox	530		Nitro -1 Ox	1132	
Nitro -2 Ox	514		Nitro -2 Ox	1116	
Di-nitro	591		Di-nitro	1193	
Di-nitro -1 Ox	575		Di-nitro -1 Ox	1177	
Di-nitro -2 Ox	559		Di-nitro -2 Ox	1161	
			Tri-nitro	1238	
			Tri-nitro -1 Ox	1222	
			Tri-nitro -2 Ox	1206	
P4: 165-PVDQ**Y**NNQNNFVHDCVNITI-185					
	peptide				
No nitration	2476			P6: 221-ESQA**YY**DGR-229	
Nitro	2521				Peptide
Nitro -1 Ox	2505			No nitration	1088
Nitro -2 Ox	2489			Nitro	1133
				Nitro -1 Ox	1117

P5: 209-VVEQMCTTQ**Y**QK-220				nitro-2ox	1101
	peptide	1metox		Di-nitro	1178
No nitration	1458	1474		Di-nitro -1 Ox	1162
Nitro	1503	1519		Di-nitro -2 Ox	1146
Nitro -1 Ox	1487	1503			
Nitro -2 Ox	1471	1487			

REFERENCES

1. Prusiner, S.B., *Prions.* Proc Natl Acad Sci U S A, 1998. **95**, 13363-83.

2. Tan, S.Y. and Pepys, M. B., *Amyloidosis.* Histopathology, 1994. **25**, 403-14.

3. Prusiner, S.B., *Novel proteinaceous infectious particles cause scrapie.* Science, 1982. **216**, 136-44.

4. Soto, C. and Castilla, J., *The controversial protein-only hypothesis of prion propagation.* Nat Med, 2004. **10**, S63-7.

5. Büeler, H., Aguzzi, A., Sailer, A., Greiner, R. A., Autenried, P., Aguet, M. and Weissmann, C., *Mice devoid of PrP are resistant to scrapie.* Cell, 1993. **73,** 1339-47.

6. Legname, G., Baskakov, I. V., Nguyen, H. B., Riesner, D., Cohen, F. E., DeArmond, S. V. and Prusiner, S. B., *Synthetic mammalian prions.* Science, 2004. **305,** 673-6.

7. Soto, C., Estrada, L., Castilla, J., *Amyloids, prions and the inherent infectious nature of misfolded protein aggregates.* Trends Biochem Sci, 2006. **31,** 150-5.

8. Castilla, J., Saá, P., Hetz, C. and Soto, C., *In vitro generation of infectious scrapie prions.* Cell, 2005. **121,** 195-206.

9. Meyer-Luehman M., Coomaraswamy, J, Bolmont, T., Kaeser, S., Schaefer, C., Kilger, E., Neuenschwander, A., Abramowski, D., Frey, P., Jaton, A. L., Vigouret, J., Paganetti, P.,Walsh, D. M., Mathews, P. M., Ghiso, J.,

Staufenbiel, M., Walker, L. C., and Jucker, M., *Exogenous induction of cerebral β-amyloidogenesis is governed by agent and host.* Science, 2006. **313,** 1781-4.

10. Harris, D. A. and True, H. A., *New insights into prion structure and toxicity.* Neuron, 2006. **50,** 353-7.

11. Weissmann, C., *The state of the prion.* Nat Rev Micro, 2004. **2**, 861-71.

12. Stahl, N., Baldwin, M.A, Teplow, D. B., Hood, L., Gibson, B. W., Burlingame, A. L. and Prusiner, S. B., *Structural studies of the scrapie prion protein using mass spectrometry and amino acid sequencing.* Biochemistry, 1993. **32**, 1991-2002.

13. Baskakov, I. V., Legname, G., Baldwin, M. A., Prusiner, S. B. and Cohen, F. E., *Pathway complexity of prion protein assembly into amyloid.* J Biol Chem, 2002. **277**, 21140-8.

14. Zahn, R., Liu, A., Luhrs, T., Riek, R., von Schroetter, C., Lopez Garcia, F., Billeter, M., Calzolai, L., Wider, G. and Wuthrich, K., *NMR solution structure of the human prion protein.* Proc Natl Acad Sci U S A, 2000. **97**, 145-50.

15. Zahn, R., Guntert, P., von Schroetter, C. and Wuthrich, K., *NMR solution structure of a varient human prion protein with two disulfide bridges.* J Mol Biol, 2003. **326**, 225-34.

16. Riek, R., Hornemann, S.,Wider, G., Billeter, M., Glockshuber, R. and Wuthrich, K., *NMR characterization of the full-length recombinant murine prion protein, mPrP(23-231).* FEBS Lett, 1997. **413**, 282-8.

17. Riek, R., Hornemann, S.,Wider, G., Billeter, M., Glockshuber, R. and

Wuthrich, K., *NMR structure of the mouse prion protein domain PrP(121-321).* Nature, 1996. **382**, 180-2.

18. Lysek, D. A., Schorn, C., Nivon, L. G., Esteve-Moya, V., Christen, B., Calzolai, L., von Schroetter, C., Friorito, F., Herrmann, T, Guntert, P. and Wuthrich, K., *Prion protein NMR structures of cats, dogs, pigs, and sheep.* Proc Natl Acad Sci U S A, 2005. **102**, 640-5.

19. Lopez Garcia, F., Zahn, R., Riek, R. and Wuthrich, K., *NMR structure of the bovine prion protein.* Proc Natl Acad Sci U S A, 2000. **97**, 8334-9.

20. Liu, H., Farr-Jones, S., Ulyanov, N. B., Llinas, M., Marqusee, S., Groth, D., Cohen, F. E., Prusiner, S. B, and James, T. L., *Solution structure of Syrian hamster prion protein rPrP(90-231).* Biochemistry, 1999. **38**, 5362-77.

21. Calzolai, L., Lysek, D. A., Perez, D. R., Guntert, P. and Wuthrich, K., *Prion protein NMR structures of chickens, turtles, and frogs.* Proc Natl Acad Sci U S A, 2005. **102**, 651-5.

22. James, T.L., Liu, H., Ulyanov, N. B., Farr-Jones, S., Zhang, H., Donne, D. G., Kaneko, K., Groth, D., Mehlhorn, I., Prusiner, S. B. and Cohen, F. E., *Solution structure of a 142-residue recombinant prion protein corresponding to the infectious fragment of the scrapie isoform.* Proc Natl Acad Sci U S A, 1997. **94**, 10086-91.

23. Haire, L.F., Whyte, S. M., Vasisht, N., Gill, A. C., Verma, C., Dodson, E. J., Dodson, G. G. and Bayley, P. M., *The crystal structure of the globular domain of sheep prion protein.* J Mol Biol, 2004. **336**, 1175-83.

24. Knaus, K. J., Morillas, M., Swietnicki, W., Malone, M., Surewicz, W. K. and Yee, V. C., *Crystal structure of the human prion protein reveals a mechanism*

for oligomerization. Nat Struct Biol, 2001. **8,** 770-4.

25. Paramithiotis, E., Pinard, M., Lawton, T., LaBoissiere, S., Leathers, V. L., Zou, W. Q., Estey, L. A., Lamontagne, J., Lehto, M. T., Kondejewski, L. H., Francoeur, G. P., Papadopoulos, M., Haghighat, A., Spatz, S. J., Head, M., Will, R., Ironside, J., O'Rourke, K., Tonelli, Q., Ledebur, H. C., Chakrabartty, A. and Cashman, N. R., *A prion protein epitope selective for the pathologically misfolded conformation.* Nat Med, 2003. **9**, 893-9.

26. Speare, J. O., Rush, T. S., 3rd, Bloom, M. E., and Caughey, B., *The role of helix 1 aspartates and salt bridges in the stability and conversion of prion protein*. J Biol Chem 2003. **278**, 12522-9.

27. Lobley, A., Whitmore, L. and Wallace, B. A., *DICHROWEB: an interactive website for the analysis of protein secondary structure from circular dichroism spectra*. Bioinformatics 2002. **18,** 211-2.

28. Whitmore, L. and Wallace, B. A., *DICHROWEB, an online server for protein secondary structure analysis from circular dichroism spectroscopic data*. Nucleic Acids Res 2005. **32,** W668-73.

29. Pace, C. N., Vajdos, F., Fee, L., Grimsley, G., and Gray, T., *How to measure and predict the molar absorption coefficient of a protein*. Protein Sci 1995. **11**, 2411-2423.

30. Koradi, R., Billeter, M., and Wuthrich, K., *MOLMOL: a program for display and analysis of macromolecular structure*s. J Mol Graph 1996. **14**, 51-5, 29-32.

31. King, P.A., Jamison, E., Strahs, D., Anderson, V. E. and Brenowitz, M., *'Footprinting' proteins on DNA with peroxonitrous acid*. Nucleic Acids Res

1993. **21**, 2473-8.

32. Gasteiger E., Hoogland C., Gattiker A., Duvaud S., Wilkins M.R., Appel R.D., Bairoch A.; *Protein Identification and Analysis Tools on the ExPASy Server;* (In) John M. Walker (ed): The Proteomics Protocols Handbook, Humana Press (2005).

33. Sarver, A., Scheffler, N. K., Shetlar, M. D., and Gibson, B. W., *Analysis of peptides and proteins containing nitrotyrosine by matrix-assisted laser desorption/ionization mass spectrometry.* J Am Soc Mass Spectrom 2001. **12**, 439-48.

34. Caughey, B. and Baron, G. S. *Prions and their partners in crime.* Nature, 2006. **443**, 803-10.

35. Vassallo, N. and Herms, J., *Cellular prion protein function in copper homeostasis and redox signaling at the synapse.* J Neuorochem, 2003. **86,** 538-44.

36. Horwich, A. and Weissman, J. S., *Deadly conformations – protein misfolding in prion diseases*. Cell, 1997. **89**, 499-510.

37. Agorogiannis, E. I., Agorogiannis, G. I., Papadimitriou, A. and Hadjigeorgiou, G. M., *Protein misfolding in neurodegenerative diseases.* Neuropath and App Neurobiol, 2004. **30,** 215-24.

38. Baskakov, I., Disterer, P., Breydo, L., Shaw, M., Gill, A., James, W. and Tahiri-Alaoui, A., *The presence of valine at residue 129 in human prion protein accelerates amyloid formation.* FEBS Lett, 2005. **579,** 2589-96.

39. Kovacs, G. G., Trabattoni, G., Hainfellner, J. A., Ironside, J. W., Knight, R. S.

G. and Budka, H., *Mutations of the prion protein gene.* J Neurol, 2002. **249,** 1567-82.

40. Reik, R., Wider, G., Billeter, M., Horneman, M., Glockshuber, R. and Wüthrich, K., *Prion protein NMR structure and familial human spongiform encephalopathies.* Proc Natl Acad Sci U S A, 1998. **95**, 11667-72.

41. Pfeiffer, S., Schmidt, K. and Mayer, B., *Dityrosine formation outcompetes tyrosine nitration at low steady-state concentrations of peroxynitrite. Implications for tyrosine modification by nitric oxide/superoxide in vivo.* J Biol Chem, 2000. **275**, 6346-52

42. Novitskaya, V., Bocharova, O. V., Bronstein, I. and Baskakov, I. V., *Amyloid Fibrils of Mammalian Prion Protein Are Highly Toxic to Cultured Cells and Primary Neurons.* J Biol Chem, 2006. **281**, 13828-36

43. Tattum, M. H., Cohen-Krausz, S., Khalili-Shirazi, A., Jackson, G. S., Orlova, E. V., Collinge, J., Clarke, A. R. and Saibil, H. R., *Elongated oligomers assemble into mammalian PrP amyloid fibrils.* J Mol Biol, 2006. **357**, 975-85.

44. Silveira, J. R., Raymond, G. J., Hughson, A. G., Race, R. E., Sim, V. L., Hayes, S. F. and Caughey, B., *The most infectious prion protein particles.* Nature, 2005. **437**, 257-61.

45. Pribic, R., von Stokkum, H. M., Chapman, D., Haris, P. I. and Bloemendal, M., *Protein secondary structure from fourier transform infrared and/or circular dichroism spectra.* Anal Biochem, 1993. **214,** 366-78.

46. Laws, D.D., Bitter, H. L., Liu, K., Ball, H. L., Kaneko, K., Wille, H., Cohen, F. E., Prusiner, S. B., Pines, A. and Wemmer, D. E., *Solid-state NMR studies of*

the secondary structure of a mutant prion protein fragment of 55 residues that induces neurodegeneration. Proc Natl Acad Sci U S A, 2001. **98**, 11686-90.

47. Khurana, R., Ionescu-Zanetti , C.,Pope , M., Li , J., Nielson , L., Ramírez-Alvarado , M., Regan , L., Fink, A. L. and Carter, S. A., *A general model for amyloid fibril assembly based on morphological studies using atomic force microscopy.* Biophys J, 2003. **85**, 1135-44.

48. Sunde, M., Serpell, L. C., Bartlam, M., Fraser, P. E., Pepys M. B. and Blake, C. F. C., *Common core structure of amyloid fibrils by synchrotron X-ray diffraction.* J Mol Biol, 1997. **273**, 729-39.

49. Caughey, B., *Interactions between prion protein isoforms: the kiss of death?,* Trends Biochem Sci, 2001. **26,** 235-42.

50. Baskakov, I. V., Aagaard, C., Mehlhorn, I., Wille, H., Groth, D., Baldwin, M. A., Prusiner, S. B., and Cohen, F. E., *Self-assembly of recombinant prion protein of 106 residues*. Biochemistry, 2002. **39**, 2792-804.

51. Flechsig, E., Shmerling, D., Hegyi, I., Raeber, A. J., Fischer, M., Cozzio, A., von Mering, C., Aguzzi, A., and Weissmann, C., *Prion protein devoid of the octapeptide repeat region restores susceptibility to scrapie in PrP knockout mice.* Neuron, 2002. **27**, 399-408.

52. Supattapone, S., Muramoto, T., Legname, G., Mehlhorn, I., Cohen, F. E., DeArmond, S. J., Prusiner, S. B., and Scott, M. R., *Identification of two prion protein regions that modify scrapie incubation time.* J Virol, 2001. **75**, 1408-13.

53. Fischer, M., Rulicke, T., Raeber, A., Sailer, A., Moser, M., Oesch, B., Brandner, S., Aguzzi, A., and Weissmann, C., *Prion protein (PrP) with amino-*

proximal deletions restoring susceptibility of PrP knockout mice to scrapie. Embo J, 1996. **15**, 1255-64.

54. Frankenfield, K. N., Powers, E. T., and Kelly, J. W., *Influence of the N-terminal domain on the aggregation properties of the prion protein.* Protein Sci, 2005. **14**, 2154-66.

55. Lawson, V. A., Priola, S. A., Wehrly, K., and Chesebro, B., *N-terminal truncation of prion protein affects both formation and conformation of abnormal protease-resistant prion protein generated in vitro.* J Biol Chem, 2001. **276**, 35265-71.

56. Lawson, V. A., Priola, S. A., Meade-White, K., Lawson, M., and Chesebro, B., *Flexible N-terminal region of prion protein influences conformation of protease-resistant prion protein isoforms associated with cross-species scrapie infection in vivo and in vitro.* J Biol Chem, 2004. **279**, 13689-95.

57. Korth, C., Stierli, B., Streit, P., Moser, M., Schaller, O., Fischer, R., Schulz-Schaeffer, W., Kretzschmar, H., Raeber, A., Braun, U., Ehrensperger, F., Hornemann, S., Glockshuber, R., Riek, R., Billeter, M., Wuthrich, K. and Oesch, B., *Prion (PrPSc)-specific epitope defined by a monoclonal antibody.* Nature, 1997. **390**, 74-7.

58. Novitskaya, V., Makarava, N., Bellon, A., Bocharova, O. V., Bronstein, I. B., Williamson, R. A. and Baskakov, I. V., *Probing the conformation of the prion protein within a single amyloid fibril using a novel immunoconformational assay*. J Biol Chem, 2006. **281**, 15536-45.

59. Caughey, B. W., Dong, A., Bhat, K. S., Ernst, D., Hayes, S. F. and Caughey, W. S., *Secondary structure analysis of the scrapie-associated protein PrP 27-30 in water by infrared spectroscopy.* Biochemistry, 1991. **30**, 7672-80.

60. Pan, K. M., Baldwin, M., Nguyen, J., Gasset, M., Serban, A., Groth, D., Mehlhorn, I., Huang, Z. W., Fletterick, R. J., Cohen, F. E., and Prusiner, S. B., *Conversion of α-helices into β-sheets features in the formation of the scrapie prion proteins.* Proc. Natl. Acad. Sci. U.S.A. **90**, 10962-66.

61. Wille, H., Michelitsch, M. D., Guenebaut, V., Supattapone, S., Serban, A., Cohen, F. E., Agard, D. A. and Prusiner, S. B., *Structural studies of the scrapie prion protein by electron crystallography.* Proc Natl Acad Sci U S A, 2002. **99**, 3563-8.

62. DeMarco, M.L. and V. Daggett, *From conversion to aggregation: protofibril formation of the prion protein.* Proc Natl Acad Sci U S A, 2004. **101**, 2293-8.

63. Govaerts, C., Wille, H., Prusiner, S. B. and Cohen, F. E., *Evidence for assembly of prions with left-handed beta-helices into trimers.* Proc Natl Acad Sci U S A, 2004. **101**, 8342-7.

64. Yang, S., Levine, H., Onuchic, J. N. and Cox, D. L., *Structure of infectious prions: stabilization by domain swapping.* Faseb J, 2005. **19**, 1778-82.

65. Malolepsza, E., Boniecki, M., Kolinski, A., and Piela, L, *Theoretical model of prion propagation: a misfolded protein induces misfolding*. *Proc Natl Acad Sci U S A* 2005. **102**, 7835-40.

66. Langedijk, J. P., Fuentes, G., Boshuizen, R., and Bonvin, A. M., *Two-rung Model of a Left-handed beta-Helix for Prions Explains Species Barrier and Strain Variation in Transmissible Spongiform Encephalopathies*. J Mol Biol 2006. **360**, 907-20.

67. Yang, S., Levine, H., Onuchic, J. N., and Cox, D. L., *Structure of infectious prions: stabilization by domain swapping*. Faseb J 2005. **19**, 1778-82.

68. DeMarco M. L., Silveira J., Caughey B., and Daggett V., *Structural Properties of Prion Protein Protofibrils and Fibrils: An Experimental Assessment of Atomic Models*. Biochemistry 2006, **45**, 15573-82.

69. Alvarez,B. and R. Radi, *Peroxynitrite reactivity with amino acids and proteins.* Amino Acids, 2003. **25**, 295-311.

70. Bruice, T.C. Gregory, M. J. and Walters, S. L., *Reactions of tetranitromethane. I. kinetics and mechanims of nitration of phenols by tetranitromethane.* J Am Chem Soc, 1968. **90**,. 1612-9.

71. Lee, S.B., Inouye, K. and Tomura, B., *The states of tyrosyl residues in thrermolysin as examined by nitration and pH-dependent ionization*. J Biochem*,* 1997. **121**, 231-7.

72. Lecomte, J.T.J. and Llinãs, M., *Characterization of the aromatic proton magnetic resonance spectrum of crambin*. Biochemistry, 1984. **23**, 4799-807.